A Nonlinear Theory for Asymmetric Sandwich Plates With a First-Order Compressible Core Impacted by a Friedlander-Type Shock Loading

Terry Hause, Ph.D.[a]

[a]Research Mechanical Engineer, U.S. Army RDECOM-TARDEC, Warren, MI 48397

Abstract

The foundation of the nonlinear theory of asymmetric anisotropic sandwich plates with a first order compressible weak orthotropic core under a Friedlander-Type explosive blast is presented. The equations of motion are developed by means of Hamilton's Principle. Within the theory, the face sheets are asymmetric while adopting the Love-Kirchoff model. In addition, the core layer is assumed to be compressible (extensible) in the transverse direction thereby capturing any wrinkling(local) or global instabilities. The theory is then simplified and applied for applicable cases of sandwich plates with symmetric orthotropic and cross-ply facings under blast loading. The governing solution is developed using the Extended-Galerkin method resulting in two coupled nonlinear second-order ordinary differential equations which are then solved using the Adaptive (variable time increments) 4^{th}-Order Runge-Kutta Method for a system of differential equations. Results are then validated for the case of a uniform pressure pulse for the incompressible core case. It is shown that reasonable agreement exists.

Key Words: Sandwich Panel; Dynamic Response; Blast; Transient Response; Friedlander; Shock Loading; Structural Response

1. Introduction

During combat situations, the structure of army military vehicles may have to withstand explosive blast loading, the residual effects of which are the blast pressure, fragmentation, and heat. Due to their outstanding characteristics, sandwich structures can be adopted in armored

Report Documentation Page

Form Approved
OMB No. 0704-0188

1. REPORT DATE	2. REPORT TYPE	3. DATES COVERED
25 JUL 2011	**N/A**	**-**

4. TITLE AND SUBTITLE	5a. CONTRACT NUMBER
A Nonlinear Theory for Asymmetric Sandwich Plates With a First-Order Compressible Core Impacted by a Friedlander-Type Shock Loading (PREPRINT)	5b. GRANT NUMBER
	5c. PROGRAM ELEMENT NUMBER

6. AUTHOR(S)	5d. PROJECT NUMBER
Terry Hause, Ph.D.	5e. TASK NUMBER
	5f. WORK UNIT NUMBER

7. PERFORMING ORGANIZATION NAME(S) AND ADDRESS(ES)	8. PERFORMING ORGANIZATION REPORT NUMBER
US Army RDECOM-TARDEC 6501 E 11 Mile Rd Warren, MI 48397-5000, USA	**22072**

9. SPONSORING/MONITORING AGENCY NAME(S) AND ADDRESS(ES)	10. SPONSOR/MONITOR'S ACRONYM(S)
US Army RDECOM-TARDEC 6501 E 11 Mile Rd Warren, MI 48397-5000, USA	**TACOM/TARDEC/RDECOM**
	11. SPONSOR/MONITOR'S REPORT NUMBER(S) **22072**

12. DISTRIBUTION/AVAILABILITY STATEMENT
Approved for public release, distribution unlimited

13. SUPPLEMENTARY NOTES
Submitted for publication in Journal of Shock and Vibration ** Disclaimer: Reference herein to any specific commercial company, product, process, or service by trade name, trademark, manufacturer, or otherwise, does not necessarily constitute or imply its endorsement, recommendation, or favoring by the United States Government or the Department of the Army (DoA). The opinions of the authors expressed herein do not necessarily state or reflect those of the United States Government or the DoA, and shall not be used for advertising or product endorsement purposes**

14. ABSTRACT

15. SUBJECT TERMS

16. SECURITY CLASSIFICATION OF:			17. LIMITATION OF ABSTRACT	18. NUMBER OF PAGES	19a. NAME OF RESPONSIBLE PERSON
a. REPORT	b. ABSTRACT	c. THIS PAGE			
unclassified	**unclassified**	**unclassified**	**SAR**	**43**	

plating and the vehicle hull structure of armored vehicles and possibly other key parts of the vehicle. Their advantages consist of, among other things, a high bending stiffness and strength to weight ratio and are lightweight in structure. These structures also provide: a) excellent thermal and sound insulation; b) increased durability under a thermo-mechanical loading environment; and c) tight thermal distortion tolerances. As a result, these structures may reveal many advantages when implemented into military armored military vehicles.

The purpose of this paper is not only for the benefit of the Army, in regards to structural applications, but also to fill in some of the gaps existing within the literature. Several papers currently existing present results, regarding the blast of sandwich panels. Among these papers several factors are considered while others are neglected. The following authors [3,4,10,11] considered blast loading of sandwich panels while neglecting the normal or transverse deformation of the core. Authors such as [5,6,7,12] have considered the deformation of the core for both under water and in-air explosive-type loading with the in-air case limited to a sonic boom and triangular pulse-type loading. In addition, the theory was limited to symmetric sandwich panels. To advance beyond this, the authors [14,15] considered the effect of a higher-order compressible core (2^{nd}-order) with an exponential decay. Within these authors works a different theoretical approach was taken as compared with [5,6,7,12]. Numerical or experimental results [2,9,13,17] have shown that the core experiences significant deformation during sudden impact. Therefore, the consideration of the deformation of the core within the governing theory is imperative. Finally, to capture a more representative model for in-air blast loading, The Friedlander-type model should be utilized. To-date the most comprehensive analytical theory presented on sandwich panels is given by [5,6,7,12]. In few of these papers [6,7,12] a nonlinear theory for symmetric anisotropic sandwich plates and shells incorporating a compressible core

exposed to under water blast and in-air blast loading has been presented with the above mentioned limitations.

This paper expands beyond the previous authors by presenting and laying the foundation for a geometrically nonlinear theory of asymmetric sandwich plates with a first order compressible core exposed to an in-air Friedlander-type explosive loading. The results are then presented for a simplification of the governing equations for the case of symmetric orthotropic and cross-ply facings.

2. Basic Assumptions and Preliminaries

Presented in Fig. 1 is a geometrical representation of a sandwich structure. The structure consists of asymmetric facings with a thick core between the facings. The face sheets are assumed to be asymmetric with respect to the global mid-surface (mid-surface of the core). The face sheet thicknesses for the top and bottom face sheets is denote by t_f^t and t_f^b, respectively, while t_c denotes the thickness of the core. A Cartesian coordinate system is placed as shown, in Fig. 1, with the transverse direction, x_3 assumed positive in the downward direction.

The tangential stiffness of the sandwich plate is assumed large which implies small tangential deformations. In contrast, large deformations can occur in the transverse direction. The face sheets are assumed incompressible while the core is assumed to be compressible in the transverse direction. Consistent with the concept of small tangential and large transverse displacements, the tangential and rotatory inertias are neglected. Where as, only the transverse inertias are considered. Finally, in addition, it is assumed that:

1. The face sheets fulfill the Love-Kirchoff assumptions and are thin compared with the core.
2. The bonding between the face sheets and the core is assumed to be perfect.

3. The kinematic boundary conditions at the interfaces between the core and the facings are satisfied.

4. The core is assumed to be a weak orthotropic transversely compressible core carrying only the transverse strains and the normal strain.

5. The shock wave pressure is uniformly distributed on the front face of the sandwich plate.

3. Kinematic Equations

3.1 Displacement Field

Consistent with standard plate and shell theory and adopting the Love-Kirchoff assumptions the displacement field for the top and bottom facings is given as:

Top Face Sheets

$$v_\alpha^t = u_\alpha^a + u_\alpha^d - \left(x_3 + \frac{t_c + t_f^t}{2} \right) u_{3,\alpha}^a - \left(x_3 + \frac{t_c + t_f^t}{2} \right) u_{3,\alpha}^d \tag{1a}$$

$$v_3^t = u_3^a + u_3^d \tag{1b}$$

Bottom Face Sheets

$$v_\alpha^b = u_\alpha^a - u_\alpha^d - \left(x_3 - \frac{t_c + t_f^b}{2} \right) u_{3,\alpha}^a + \left(x_3 - \frac{t_c + t_f^b}{2} \right) u_{3,\alpha}^d \tag{2a}$$

$$v_3^b = u_3^a - u_3^d \tag{2b}$$

In the above equations, the Greek indices have the range 1, 2, while the Latin indices have the range 1, 2, 3 and unless otherwise stated, Einstein's summation convention over the repeated indices is assumed. Also, $(\cdot)_{,i}$ denotes partial differentiation with respect to the coordinates x_i, while superscripts *t* and *b* indicate the association with the top and bottom facings respectively.

A second order power series is assumed for the core tangential displacements while a first order polynomial is assumed for the core transverse displacement [5,6,7,12]. With this in hand, the core displacement field is represented in compact notation as

$$v_1^c = \sum_0^2 u_i^c z^i \,, \quad v_2^c = \sum_0^2 v_i^c z^i \,, \quad v_3^c = \sum_0^1 w_i^c z^i \tag{3a-c}$$

Satisfying the interfacial continuity conditions at the interfaces between the facings and the core, namely:

Top face sheet/core interface $(x_3 = -t_c/2)$

$$v_\alpha^c = v_\alpha^t, \quad v_3^c = v_3^t \tag{4a,b}$$

Bottom face sheet/core interface $(x_3 = t_c/2)$

$$v_\alpha^c = v_\alpha^b, \quad v_3^c = v_3^b \tag{5a,b}$$

Results in the following displacement field for the core.

$$\begin{aligned} v_\alpha^c = {} & u_\alpha^a - \left(\frac{t_f^t - t_f^b}{4}\right) u_{3,\alpha}^a - \left(\frac{t_f^t + t_f^b}{4}\right) u_{3,\alpha}^d - \frac{2x_3}{t_c} u_\alpha^d + \left(\frac{t_f^t + t_f^b}{2t_c}\right) x_3 u_{3,\alpha}^a + \left(\frac{t_f^t - t_f^b}{2t_c}\right) x_3 u_{3,\alpha}^d \\ & + \left(\frac{4x_3^2}{t_c^2} - 1\right) \Phi_\alpha^c \end{aligned} \tag{6a}$$

$$v_3^c(x, y, z, t) = u_3^a - \frac{2x_3}{t_c} u_3^d \tag{6b}$$

For the special case of symmetric facings with respect to the global mid-surface, $t_f^t = t_f^b = t^f$. In Equations (1a,b), (2a,b), and (6a,b) the displacement functions

$$u_i^a = \frac{1}{2}(u_i^t + u_i^b), \quad u_i^d = \frac{1}{2}(u_i^t - u_i^b) \tag{7a,b}$$

represent the average and the half difference of the face sheet mid-surface displacements while, the core displacements, Φ_α^c represent warping functions of the core.

3.2 Non-Linear Strain-Displacement Relationships

The strain-displacement relationships given by the Lagrangian Strain-Displacement Relationships used in conjunction with the Von-Karman assumptions is given in compact indicial notation as:

$$2\gamma_{ij} = \upsilon_{i,j} + \upsilon_{j,i} + \upsilon_{3,i}\upsilon_{3,j} \tag{8a}$$

In expanded form, they are given as

$$\gamma_{11} = \upsilon_{1,1} + \frac{1}{2}(\upsilon_{3,1})^2 \tag{8b}$$

$$\gamma_{22} = \upsilon_{2,2} + \frac{1}{2}(\upsilon_{3,2})^2 \tag{8c}$$

$$\gamma_{33} = \upsilon_{3,3} + \frac{1}{2}(\upsilon_{3,3})^2 \tag{8d}$$

$$\gamma_{23} = \frac{1}{2}(\upsilon_{2,3} + \upsilon_{3,2}) + \frac{1}{2}\upsilon_{3,2}\upsilon_{3,3} \tag{8e}$$

$$\gamma_{13} = \frac{1}{2}(\upsilon_{1,3} + \upsilon_{3,1}) + \frac{1}{2}\upsilon_{3,1}\upsilon_{3,3} \tag{8f}$$

$$\gamma_{12} = \frac{1}{2}(\upsilon_{1,2} + \upsilon_{2,1}) + \frac{1}{2}\upsilon_{3,1}\upsilon_{3,2} \tag{8g}$$

Substituting the displacement relationships, Eqs. (1a,b), (2a,b) and (6a,b) into the nonlinear strain-displacement relationships, for the individual layers of the structure (top, bottom, and core layers), results in:

$$\gamma^t_{\alpha\beta} = \bar{\gamma}^a_{\alpha\beta} + \bar{\gamma}^d_{\alpha\beta} + \left(x_3 + \frac{t_c + t^t_f}{2}\right)\kappa^a_{\alpha\beta} + \left(x_3 + \frac{t_c + t^t_f}{2}\right)\kappa^d_{\alpha\beta} \tag{9a}$$

and

$$\gamma_{\alpha\beta}^{b} = \bar{\gamma}_{\alpha\beta}^{a} - \bar{\gamma}_{\alpha\beta}^{d} + \left(x_3 - \frac{t_c + t_f^b}{2} \right) \kappa_{\alpha\beta}^{a} - \left(x_3 - \frac{t_c + t_f^b}{2} \right) \kappa_{\alpha\beta}^{d} \tag{9b}$$

Where

$$\bar{\gamma}_{\alpha\beta}^{a} = \frac{1}{2}(\bar{\gamma}_{\alpha\beta}^{t} + \bar{\gamma}_{\alpha\beta}^{b}), \quad \bar{\gamma}_{\alpha\beta}^{d} = \frac{1}{2}(\bar{\gamma}_{\alpha\beta}^{t} - \bar{\gamma}_{\alpha\beta}^{b}) \tag{10a}$$

and

$$\kappa_{\alpha\beta}^{a} = \frac{1}{2}(\kappa_{\alpha\beta}^{t} + \kappa_{\alpha\beta}^{b}), \quad \kappa_{\alpha\beta}^{d} = \frac{1}{2}(\kappa_{\alpha\beta}^{t} - \kappa_{\alpha\beta}^{b}) \tag{10b}$$

In the above expressions, $\bar{\gamma}_{\alpha\beta}^{(a,d)}$ are referred to as the average and half difference of tangential or membrane strains of the top and bottom facings; while, $\kappa_{\alpha\beta}^{(a,d)}$ are referred to as the average and half difference of the bending strains of the top and bottom facings. The expressions for the membrane and bending strains are provided in Appendix A.

For the core, the strain-displacement relationships take the form

$$\gamma_{i3}^{c} = \bar{\gamma}_{i3}^{c} + z\kappa_{i3}^{c} \quad , \tag{11}$$

In these expressions, $\bar{\gamma}_{i3}^{c}$ and κ_{i3}^{c} are the membrane and bending strains, respectively. These expressions are also provided in Appendix A.

4. Constitutive Equations

Both the top and bottom face sheets are considered to be constructed from unidirectional fiber reinforced anisotropic laminated composites, the axes of orthotropy not necessarily being coincident with the geometrical axes (x_1, x_2). The stress-strain relationships for each lamina of the facings becomes

$$\begin{Bmatrix} \tau_{11} \\ \tau_{22} \\ \tau_{12} \end{Bmatrix} = \begin{bmatrix} \overline{Q}_{11} & \overline{Q}_{12} & \overline{Q}_{16} \\ & \overline{Q}_{22} & \overline{Q}_{26} \\ \text{Sym} & & \overline{Q}_{66} \end{bmatrix} \begin{Bmatrix} \gamma_{11} \\ \gamma_{22} \\ 2\gamma_{12} \end{Bmatrix} \tag{12}$$

Where

$\overline{Q}_{ij}$ for $i, j = (1, 2, 6)$ are the *Transformed plane-stress reduced stiffness measures*. See Reddy [16].

The stress-strain relationships for the orthotropic core with the geometrical and material axes coincident are expressed as

$$\tau_{33}^{c} = E^{c}\gamma_{33}^{c}, \quad \tau_{13}^{c} = G_{13}^{c}\gamma_{13}^{c}, \quad \tau_{23}^{c} = G_{23}^{c}\gamma_{23}^{c}. \tag{13a-c}$$

5. Equations of Motion and Boundary Conditions

An energy approach is taken to determine the equations of motion and as a by product, the boundary conditions. Letting U represent the strain energy, W represent the work done by external forces, and T represent the kinetic energy, Hamilton's Variational Principle can be expressed as

$$\int_{t_0}^{t_1} (\delta U - \delta W - \delta T) dt = 0. \tag{14}$$

It should be mentioned that hamilton's principle is valid for both elastic and elastic-plastic theoretical models. Assuming a weak compressible core, the variation of the strain energy and work can be written as

$$\delta U = \int_{A} \left(\int_{-t_c/2-t_f^t}^{-t_c/2} \tau_{\alpha\beta}^{t} \delta\gamma_{\alpha\beta}^{t} dx_3 + \int_{-t_c/2}^{+t_c/2} \tau_{i3}^{c} \delta\gamma_{i3}^{c} dx_3 + \int_{t_c/2}^{t_c/2+t_f^b} \tau_{\alpha\beta}^{b} \delta\gamma_{\alpha\beta}^{b} dx_3 \right) dA \tag{15}$$

Where τ_{ij} are the tensorial components of the second Piola-Kirchoff stress tensor, while A is attributed to the area of the sandwich plate. With respect to the work done by external loads, only

the external work done by the transverse loading due to the explosive pressure pulse as well as energy loss due to structural damping will be considered. All work due to tangential loadings will be neglected. The δW takes the form

$$\delta W = \int_A \left(\hat{q}_3^t(x_1, x_2, t)\delta v_3^t + \hat{q}_3^b(x_1, x_2, t)\delta v_3^b - 2C^t \dot{v}_3^t \delta v_3^t - 2C^c \dot{v}_3^c \delta v_3^c - 2C^b \dot{v}_3^b \delta v_3^b \right) dA \tag{16}$$

where $q^t(x_1, x_2, t)$ denotes the transverse pressure loading from a spherical air-blast and C is the structural damping coefficient per unit area of the plate. Discarding tangential and rotatory inertia effects, the variation of the kinetic energy can be written as

$$\int_{t_0}^{t_1} \delta T dt = \int_{t_0}^{t_1} \int_A - \left(\int_{-t_c/2-t_f^t}^{-t_c/2} \rho_f^t \ddot{v}_3^t \delta v_3^t dx_3 + \int_{-t_c/2}^{t_c/2} \rho^c \ddot{v}_3^c \delta v_3^c dx_3 + \int_{t_c/2}^{t_c/2+t_f^b} \rho_f^b \ddot{v}_3^b \delta v_3^b dx_3 \right) dA dt \tag{17}$$

Where ρ^c and ρ_f^t, ρ_f^b, are the mass densities of the core and the top and bottom face sheets, respectively, and $\ddot{v}$ denotes the transverse acceleration.

The equations of motion, in terms of the global stress resultants and stress couples are obtained by substituting Eqs. (15) – (17) and the strain-displacement relationships, Eqs. (9) – (11), while utilizing the definitions of the stress resultants and stress couples into Hamilton's Equation (14), while collecting the coefficients of each of the virtual displacements, integrating by parts where ever feasible, and invoking the independent and arbitrary character of the virtual displacements results in the following nonlinear equations of motion along with the corresponding boundary conditions.

$$\delta u_\alpha^a : \quad N_{\alpha\beta,\beta}^a = 0 \tag{18a}$$

$$\delta u_\alpha^d : \quad N_{\alpha\beta,\beta}^d + \frac{N_{\alpha 3}^c}{t_c} = 0 \tag{18b}$$

$$\delta \Phi_\alpha^c : \quad M_{\alpha 3}^c = 0 \tag{18c}$$

$$\delta u_3^a:\ u_{3,\alpha\beta}^a N_{\alpha\beta}^a + M_{\alpha\beta,\alpha\beta}^a + u_{3,\alpha\beta}^d N_{\alpha\beta}^d + \frac{1}{t_c}\left(\frac{2t_c + t_f^t + t_f^b}{4} - u_3^d\right)N_{\alpha 3,\alpha}^a - \frac{2}{t_c}u_{3,\alpha}^d N_{\alpha 3}^c$$
$$-\left(\frac{t_f^t\rho^t + t_f^b\rho^b + t_c\rho^c}{2}\right)\ddot{u}_3^a - \left(\frac{t_f^t\rho^t - t_f^b\rho^b}{2}\right)\ddot{u}_3^d - \left(\frac{C^t + C^b}{2} + C^c\right)\dot{u}_3^a \tag{18d}$$
$$-\left(\frac{C^t - C^b}{2}\right)\dot{u}_3^d + \frac{\hat{q}_3^t + \hat{q}_3^b}{2} = 0$$

$$\delta u_3^d:\ u_{3,\alpha\beta}^a N_{\alpha\beta}^d + M_{\alpha\beta,\alpha\beta}^d + u_{3,\alpha\beta}^d N_{\alpha\beta}^a + \left(1 - \frac{2}{t_c}u_3^d\right)N_{33}^c + \left(\frac{t_f^t - t_f^b}{4t_c}\right)N_{\alpha 3,\alpha}^c$$
$$-\frac{1}{2}\left(t_f^t\rho^t + t_f^b\rho^b + \frac{t_c\rho^c}{3}\right)\ddot{u}_3^d - \left(\frac{t_f^t\rho^t - t_f^b\rho^b}{2}\right)\ddot{u}_3^a - \left(\frac{C^t + C^b}{2}\right)\dot{u}_3^d - \left(\frac{C^t - C^b}{2}\right)\dot{u}_3^a \tag{18e}$$
$$+\frac{\hat{q}_3^t - \hat{q}_3^b}{2} = 0$$

In the above equations, the global stress resultants and stress couples are defined as

$$\left(N_{\alpha\beta}^a, M_{\alpha\beta}^a\right) = \frac{1}{2}\left\{\left(N_{\alpha\beta}^t + N_{\alpha\beta}^b\right), \left(M_{\alpha\beta}^t + M_{\alpha\beta}^b\right)\right\} \tag{19a}$$

$$\left(N_{\alpha\beta}^d, M_{\alpha\beta}^d\right) = \frac{1}{2}\left\{\left(N_{\alpha\beta}^t - N_{\alpha\beta}^b\right), \left(M_{\alpha\beta}^t - M_{\alpha\beta}^b\right)\right\} \tag{19b}$$

Where the local stress resultants and stress couples are given as:

$$\left\{N_{\alpha\beta}^t,\ M_{\alpha\beta}^t\right\} = \int_{-t_c/2-t_f^t}^{-t_c/2} \tau_{\alpha\beta}^t \left\{1, \left(x_3 + \frac{t_c + t_f^t}{2}\right)\right\} dx_3 \tag{20a}$$

$$\left\{N_{\alpha\beta}^b,\ M_{\alpha\beta}^b\right\} = \int_{t_c/2}^{t_c/2+t_f^b} \tau_{\alpha\beta}^b \left\{1, \left(x_3 - \frac{t_c + t_f^b}{2}\right)\right\} dx_3 \tag{20b}$$

$$\left\{N_{i3}^c,\ M_{i3}^c\right\} = \int_{-t_c/2}^{-t_c/2} \tau_{i3}^c (1, x_3) dx_3\ , \quad (i = 1, 2, 3) \tag{20c}$$

The local stress resultants and stress couples can be expressed in terms of the displacements by substituting the corresponding constitutive relationships, Eqs. (12), (13a-c) along with the strain-displacement relationships, Eqs. (9) – (11) into Eqs. (14) - (16). This results in

Top face:

$$\begin{pmatrix} N_{11}^t \\ N_{22}^t \\ N_{12}^t \\ M_{11}^t \\ M_{22}^t \\ M_{12}^t \end{pmatrix} = \begin{pmatrix} A_{11}^t & A_{12}^t & A_{16}^t & B_{11}^t & B_{12}^t & B_{16}^t \\ & A_{22}^t & A_{26}^t & B_{12}^t & B_{22}^t & B_{26}^t \\ & & A_{66}^t & B_{16}^t & B_{26}^t & B_{66}^t \\ & & & D_{11}^t & D_{12}^t & D_{16}^t \\ & & & & D_{22}^t & D_{26}^t \\ \text{Sym} & & & & & D_{66}^t \end{pmatrix} \begin{pmatrix} \bar{\gamma}_{11}^t \\ \bar{\gamma}_{22}^t \\ 2\bar{\gamma}_{12}^t \\ \kappa_{11}^t \\ \kappa_{22}^t \\ 2\kappa_{12}^t \end{pmatrix} \tag{21a}$$

Bottom face:

$$\begin{pmatrix} N_{11}^b \\ N_{22}^b \\ N_{12}^b \\ M_{11}^b \\ M_{22}^b \\ M_{12}^b \end{pmatrix} = \begin{pmatrix} A_{11}^b & A_{12}^b & A_{16}^b & B_{11}^b & B_{12}^b & B_{16}^b \\ & A_{22}^b & A_{26}^b & B_{12}^b & B_{22}^b & B_{26}^b \\ & & A_{66}^b & B_{16}^b & B_{26}^b & B_{66}^b \\ & & & D_{11}^b & D_{12}^b & D_{16}^b \\ & & & & D_{22}^b & D_{26}^b \\ \text{Sym} & & & & & D_{66}^b \end{pmatrix} \begin{pmatrix} \bar{\gamma}_{11}^b \\ \bar{\gamma}_{22}^b \\ 2\bar{\gamma}_{12}^b \\ \kappa_{11}^b \\ \kappa_{22}^b \\ 2\kappa_{12}^b \end{pmatrix} \tag{21b}$$

Where,

$$\left(A_{ij}^t, B_{ij}^t, D_{ij}^t\right) = \int_{-t_c/2-t_f^t}^{-t_c/2} \overline{Q}_{ij}^t \left\{1, \left(x_3 + \frac{t_c + t_f^t}{2}\right), \left(x_3 + \frac{t_c + t_f^t}{2}\right)^2\right\} dx_3 \tag{22}$$

And

$$\left(A_{ij}^b, B_{ij}^b, D_{ij}^b\right) = \int_{t_c/2}^{t_c/2+t_f^b} \overline{Q}_{ij}^b \left\{1, \left(x_3 - \frac{t_c + t_f^b}{2}\right), \left(x_3 - \frac{t_c + t_f^b}{2}\right)^2\right\} dx_3 \tag{23}$$

For the special case of symmetric facings with respect to the local mid-surfaces, $[B_{ij}^{(t,b)}]=0$. The stress resultants in terms of the strain deformation components of the core take the form

$$\begin{pmatrix} N_{33}^c \\ N_{23}^c \\ N_{13}^c \end{pmatrix} = \begin{pmatrix} A_{33}^c & 0 & 0 \\ 0 & A_{44}^c & 0 \\ 0 & 0 & A_{55}^c \end{pmatrix} \begin{pmatrix} \bar{\gamma}_{33}^c \\ 2\bar{\gamma}_{23}^c \\ 2\bar{\gamma}_{13}^c \end{pmatrix}, \quad \begin{pmatrix} M_{33}^c \\ M_{23}^c \\ M_{13}^c \end{pmatrix} = \begin{pmatrix} D_{33}^c & 0 & 0 \\ 0 & D_{44}^c & 0 \\ 0 & 0 & D_{55}^c \end{pmatrix} \begin{pmatrix} \kappa_{33}^c \\ 2\kappa_{23}^c \\ 2\kappa_{13}^c \end{pmatrix} \tag{24a,b}$$

The core stiffness's are given by

$$(A_{(ii)}^c, D_{(ii)}^c) = \int_{-t_c/2}^{+t_c/2} Q_{(ii)}^c (1, x_3^2) dx_3 , \qquad i = (3, 4, 5) \tag{25}$$

Where no summation, with respect to the repeated indices, is assumed. The core transverse and normal moduli are given as:

$$Q_{33}^c = E^c, \quad Q_{44}^c = G_{yz}^c, \quad Q_{55}^c = G_{xz}^c \tag{26}$$

The corresponding boundary conditions are given as:

$$u_n^a = 0 \qquad \text{or} \quad N_{nn}^a = 0 \tag{27a}$$

$$u_t^a = 0 \qquad \text{or} \quad N_{nt}^a = 0 \tag{27b}$$

$$u_n^d = 0 \qquad \text{or} \quad N_{nn}^d = 0 \tag{27c}$$

$$u_t^d = 0 \qquad \text{or} \quad N_{nt}^d = 0 \tag{27d}$$

$$u_3^a = 0 \qquad \text{or} \quad u_{3,n}^a N_{nn}^a + u_{3,t}^a N_{nt}^a + u_{3,n}^d N_{nn}^d + u_{3,t}^d N_{nt}^d + M_{nn,n}^a + 2M_{nt,t}^a + \frac{1}{t_c}\left(\frac{2t_c + t_f^t + t_f^b}{4} - u_3^d\right) N_{n3}^c = 0 \tag{27e}$$

$$u_3^d = 0 \qquad \text{or} \quad u_{3,n}^a N_{nn}^d + u_{3,t}^a N_{nt}^d + u_{3,n}^d N_{nn}^a + u_{3,t}^d N_{nt}^a + M_{nn,n}^d + 2M_{nt,t}^d + \left(\frac{t_f^t - t_f^b}{4t_c}\right) N_{n3}^c \tag{27f}$$

$$= 0$$

$$u^a_{3,n} = 0 \qquad \text{or} \quad M^a_{nn} = 0 \tag{27g}$$

$$u^d_{3,n} = 0 \qquad \text{or} \quad M^d_{nn} = 0 \tag{27h}$$

Where *n* and *t* are the normal and tangential directions to the boundary. When $n = 1$, $t = 2$, and when $n = 2$, $t = 1$. The quantities with an overcaret represent the prescribed quantities on the boundary.

For the case of *simply supported boundary conditions*, the boundary conditions become:

Along the edges $x_n = (0, L_n)$

$$N^a_{nn} = N^d_{nn} = N^a_{nt} = N^d_{nt} = M^a_{nn} = M^d_{nn} = u^a_3 = u^d_3 = 0 \tag{28a-h}$$

6. Spherical in-Air blast Loading of the Friedlander-Type

With the ever increasing demands for increased safety for the warfighter in the field to operate structurally sound vehicles in the event of an IED or some other type of explosive, it is imperative that an understanding of the structural response of various components within military combat vehicles under an explosive blast be understood so that measures can be taken from a design standpoint to ensure the durability and survivability of these components. To begin to achieve this understanding, the type of explosive loading considered here is a free in-air spherical air burst. Such an explosion creates a spherical shock wave which travels radially outward in all directions with diminishing velocity. The form of the incident blast wave from a spherical charge is shown in Fig. 2. Where q_{S0} is the peak overpressure above ambient pressure, q_0 is the ambient pressure, t_a is the time of arrival, t_p is the positive phase duration of the blast wave, and t is the time. The waveform shown in Fig. 2. is given by an expression known as the Friedlander equation and is given as

$$q_t(t) = (q_{S0} - q_0)[1 - (t - t_a)/t_p]\exp[-\alpha(t - t_a)/t_p] \tag{29a}$$

Where,

$$q_{S0} = 1772/Z^3 - 114/Z^2 + 108/Z \tag{29b}$$

In Eq. (29b), Z is known as the scaled distance given by $z = R/W^{1/3}$ with R being the standoff distance in meters and W being the equivalent charge weight of TNT in terms of kilograms. Also, α is known as the decay parameter which is determined by adjustment to a pressure curve from a blast test.

For the conditions of standard temperature and pressure (STP) at sea level, the time of arrival t_a and the positive phase duration t_p can be determined from [8]

$$t/t_1 = R/R_1 = (W/W_1)^{1/3} \tag{30}$$

Where t_1 represents either the arrival time or positive phase duration for a reference explosion of charge weight W_1, and t represents either the arrival time or positive phase duration for any explosion of charge weight W. The determination of the standoff distance for any charge weight W follows a similar reasoning. The application of these relationships is known as cube root scaling. It should be understood that in applying these relationships that the standoff distances are themselves scaled according to the cube root law.

7. Solution Methodology

Up to this point, the overall governing system of equations developed, applies to asymmetric sandwich plates both locally and globally with laminated composite facings and a weak transversely orthotropic first-order compressible core under transverse loading. For the purpose or scope of this paper, the equations will be simplified for the case of symmetric sandwich plates

with orthotropic and cross-ply facings with a transversely orthotropic compressible core under a Friedlander-type of explosive transverse loading.

6.1 Special Case: Symmetric orthotropic single layer facings

For this special case, $t_f^t = t_f^b = t^f$. In fulfillment of the geometric boundary conditions, a suitable representation for u_3^a, and u_3^d is given by:

$$u_3^a = w_{mn}^a(t)\sin(\lambda_m x_1)\sin(\mu_n x_2) \tag{31a}$$

$$u_3^d = w_{mn}^d(t)\sin(\lambda_m x_1)\sin(\mu_n x_2) \tag{31b}$$

where $\lambda_m = m\pi/L_1$, $\mu_n = n\pi/L_2$. *m* and *n* are the number of sine half-waves in the corresponding directions whereas $w_{mn}^a(t)$ and $w_{mn}^d(t)$ denote the modal amplitudes as a function of time of the transverse displacement functions. The transverse loading is represented by

$$q_t(x_1, x_2, t) = q_{mn}(t)\sin(\lambda_m x_1)\sin(\mu_n x_2), \tag{32a}$$

which implies through integration of both sides over the plate area that

$$q_{mn}(t) = \frac{4}{L_1 L_2}\int_0^{L_2}\int_0^{L_1} q_t(x_1, x_2, t)\sin(\lambda_m x_1)\sin(\mu_n x_2)dx_1 dx_2 \ . \tag{32b}$$

Letting,

$$q_t(x_1, x_2, t) = q_t(t) = (q_{S0} - q_0)[1-(t-t_a)/t_p]\exp[-\alpha(t-t_a)/t_p] \tag{32c}$$

and integrating gives

$$q_{mn}(t) = \frac{16 q_t(t)}{mn\pi^2} \tag{32d}$$

The chosen solution methodology of the governing system of equations is the Extended Galerkin method. With this in mind, the first two equations of motion, Eqs. (18a), can be satisfied by assuming a stress potential approach with the following representations.

$$N_{\alpha\beta} = c_{\alpha\omega} c_{\beta\rho} \varphi_{,\omega\rho} \tag{33}$$

where $c_{\alpha\beta}$ denotes the 2-D permutation symbol. This introduces another variable in the governing system of equations that requires determination. The determination comes from a compatibility condition or equation. The compatibility equation can be obtained from the membrane or tangential strains from the strain-displacement relationships, Eqs. (9,10) and Appendix A by eliminating the in-plane displacements. This results in:

$$\bar{\gamma}^a_{11,22} - 2\bar{\gamma}^a_{12,12} + \bar{\gamma}^a_{22,11} = (u^a_{3,12})^2 + (u^d_{3,12})^2 - u^a_{3,11}u^a_{3,22} - u^d_{3,11}u^d_{3,22} \tag{34}$$

Keeping in mind that for symmetric orthotropic and or cross-ply facings $[B^{(t,b)}_{ij}] = 0$ and $A^f_{\alpha 6}, D^f_{\alpha 6} = 0$, the following global constitutive relationships can be determined by utilizing Eqs. (19a,b) and (21a,b) which are given as

$$\begin{pmatrix} N^a_{11} \\ N^a_{22} \\ N^a_{12} \end{pmatrix} = \begin{pmatrix} A^f_{11} & A^f_{12} & 0 \\ A^f_{12} & A^f_{22} & 0 \\ 0 & 0 & A^f_{66} \end{pmatrix} \begin{pmatrix} \bar{\gamma}^a_{11} \\ \bar{\gamma}^a_{22} \\ 2\bar{\gamma}^a_{12} \end{pmatrix}, \quad \begin{pmatrix} N^d_{11} \\ N^d_{22} \\ N^d_{12} \end{pmatrix} = \begin{pmatrix} A^f_{11} & A^f_{12} & 0 \\ A^f_{12} & A^f_{22} & 0 \\ 0 & 0 & A^f_{66} \end{pmatrix} \begin{pmatrix} \bar{\gamma}^d_{11} \\ \bar{\gamma}^d_{22} \\ 2\bar{\gamma}^d_{12} \end{pmatrix} \tag{35a,b}$$

where $A^f_{ij} = A^t_{ij} = A^b_{ij}$. By performing a matrix inversion in Eq. (35a), utilizing Eqs. (33), and substituting into Eq. (34) provides the following nonlinear partial differential equation in terms of the Airy's stress potential.

$$A^*_{11}\varphi_{,2222} + (2A^*_{12} + A^*_{66})\varphi_{,1122} + A^*_{22}\varphi_{,1111} = (u^a_{3,12})^2 + (u^d_{3,12})^2 - u^a_{3,11}u^a_{3,22} - u^d_{3,11}u^d_{3,22} \tag{36}$$

where $[A^*_{ij}] = [A^f_{ij}]^{-1}$. From Eq. (36) φ can be determined by assuming the following general functional form then substitituting into Eq. (36), and comparing coefficients.

$$\varphi(x_1,x_2,t) = (w_{mn}^a)^2 C_1 \cos(2\lambda_m x_1) + (w_{mn}^a)^2 C_2 \cos(2\mu_n x_2) + (w_{mn}^d)^2 C_3 \cos(2\lambda_m x_1) + (w_{mn}^d)^2 C_4 \cos(2\mu_n x_2) \tag{37}$$

where the expressions for, C_1, C_2,C_3, and C_4 are provided in Appendix B. With the Airy's Stress potential function in hand along with Eqs. (34a,b), (33), the first two relationships of Eq. (35a), and the expressions for the membrane strain components from Appendix A, yields a system of two coupled inhomogeneous partial differential equations in terms of u_1^a and u_2^a . By assuming the following two general solutions for u_1^a and u_2^a, shown below in Eqs. (38a-b) and substituting these expressions into the coupled partial differential equations, and comparing coefficients gives.

$$u_1^a(x_1,x_2,t) = \left((w_{mn}^a)^2 + (w_{mn}^d)^2\right)D_1 x_1 + \left((w_{mn}^a)^2 + (w_{mn}^d)^2\right)D_2 \sin(2\lambda_m x_1) + \left((w_{mn}^a)^2 + (w_{mn}^d)^2\right)D_3 \sin(2\lambda_m x_1)\cos(2\mu_n x_2) \tag{38a}$$

$$u_2^a(x_1,x_2,t) = \left((w_{mn}^a)^2 + (w_{mn}^d)^2\right)E_1 x_2 + \left((w_{mn}^a)^2 + (w_{mn}^d)^2\right)E_2 \sin(2\mu_n x_2) + \left((w_{mn}^a)^2 + (w_{mn}^d)^2\right)E_3 \cos(2\lambda_m x_1)\sin(2\mu_n x_2) \tag{38b}$$

Where the constants $D_1 - D_3$ and $E_1 - E_3$ are provided in Appendix B.

By expressing the third and fourth equations of motion, Eqs. (18b) in terms of displacements utilizing Eqs. (24) and (35b) with the corresponding strain deformation components from Appendix A two coupled partial differential equations result. These coupled partial differential equations can be solved simultaneously by assuming u_1^d, and u_2^d in the following form.

$$u_1^d(x_1,x_2,t) = w_{mn}^a w_{mn}^d A_1 \sin(2\lambda_m x_1) + w_{mn}^a w_{mn}^d A_2 \sin(2\lambda_m x_1)\cos(2\mu_n x_2) + w_{mn}^a A_3 \cos(\lambda_m x_1)\sin(\mu_n x_2) \tag{39a}$$

$$u_2^d(x_1,x_2,t) = w_{mn}^a w_{mn}^d B_1 \sin(2\mu_n x_2) + w_{mn}^a w_{mn}^d B_2 \cos(2\lambda_m x_1)\sin(2\mu_n x_2) + w_{mn}^a B_3 \sin(\lambda_m x_1)\cos(\mu_n x_2) \tag{39b}$$

Then substituting these displacement representations into the coupled partial differential equations and comparing coefficients. These coefficients $A_1 - A_3$ and $B_1 - B_3$ are provided in Appendix B.

Utilizing the core deformation components κ_{i3}^c from Appendix A in conjunction with the constitutive equations (24b) the fifth and sixth equations of motion (18c) can be expressed in terms of displacements. The result is two simultaneous algebraic equations allowing for the determination of Φ_α^c. The result is given as

$$\Phi_\alpha^c = \frac{t_c}{4} u_{3,\alpha}^d - \frac{1}{2} u_3^d u_{3,\alpha}^d \tag{40}$$

This relationship reduces an 9 parameter system (u_i^a, u_i^d, Φ_α^c, and φ) to a 7 parameter system (u_i^a, u_i^d, and φ) by eliminating the variable Φ_α^c from the governing system. At this point the first six equations of motion are satisfied and all displacement functions are known. These displacement functions Eqs. (31a,b), (37), (38a,b), (39a,b), and (40) satisfy all of the transverse geometric boundary conditions and the boundary conditions with respect to the stress couples, M_{nn}^a and M_{nn}^d. The remaining boundary conditions with respect to the tangential stress resultants, $N_{nn}^a, N_{nt}^{a,}, N_{nn}^d, N_{nt}^d$ will be satisfied in an integral average sense through application of the Extended-Galerkin Method. The only unknowns at this point are the modal amplitudes, $w_{mn}^a(t)$ and $w_{mn}^d(t)$ which are determined by means of the extended Galerkin Method, (Hause et

al [2,3]). By expressing the last two unfulfilled equations of motion, Eqs. (18d,e), and the unfulfilled boundary conditions in terms of displacements through the use of Eqs. (33), (35a,b), (37), (38a,b), and (39a,b) and retaining these expressions in Hamilton's Energy Functional carrying out the indicated integrations and collecting the coefficients of the modal amplitudes w_{mn}^a and w_{mn}^d keeping in mind that the variations of δw_{mn}^a and δw_{mn}^d are arbitrary and independent from each other and that the corresponding coefficients must vanish results in two nonlinear coupled second order ordinary differential equations in terms of the modal amplitudes which is solved using the Adaptive 4th-order Runge-Kutta method for a system of differential equations. This sytem of differential equations is given as:

$$m_1 \ddot{w}_{mn}^a + C\dot{w}_{mn}^a + C_{10}^a w_{mn}^a + C_{11}^a w_{mn}^a w_{mn}^d + C_{12}^a w_{mn}^a (w_{mn}^d)^2 + C_{30}^a (w_{mn}^a)^3 = \frac{q_{mn}}{2} \tag{41a}$$

$$m_2 \ddot{w}_{mn}^d + C\dot{w}_{mn}^d + C_{01}^d w_{mn}^d + C_{02}^d (w_{mn}^d)^2 + C_{03}^d (w_{mn}^d)^3 + C_{20}^d (w_{mn}^a)^2 + C_{21}^d (w_{mn}^a)^2 w_{mn}^d = \frac{q_{mn}}{2} \tag{41b}$$

The coefficients $C_{10} - C_{12}, C_{30}, C_{01} - C_{03}, C_{20}, C_{21}$ are expressions which depend on the material and geometrical properties of the structure which are provided in Appendix C. C is the damping coefficient, while q_{mn} is the amplitude of the transverse loading.

8. Results and Discussion

Results are presented next for the dynamic response of simply supported sandwich plates along all four edges and freely movable under various fixed or varied geometrical and material properties of the structure exposed to blast loading to develop a deeper understanding of what effect these parameters play in the behavior of the structure. The results consist of two parts. The first part is concerned with comparisons/validations and the second part is concerned with the current or present results produced from the governing theory.

8.1 Validation

To validate the results, The dynamic response of a sandwich plate with an incompressible weak core impacted by a uniform pressure pulse was chosen from R.S. Alwar et al [1]. The sandwich plate is assumed to be simply supported and freely movable along all four edges. The uniform pressure pulse is given by $q_{mn}(t) = 16q_0/\pi^2 mn$ where q_0 is the uniform pressure.

The geometrical and material properties used for the validation are given for the face-sheets as, $L_1 = L_2 = 1.83\ \text{m}$, $t_f = 0.000406\ \text{m}$, $E_1^f = 68.96\ (\text{GPa})$, $E_2^f = 68.96\ (\text{GPa})$, $G_{12}^f = 25.92\ (\text{GPa})$, $v_{12}^f = 0.33$, and $\rho_f = 2768.38\ (\text{Kg/m}^3)$. The corresponding properties for the core are provided as $t_c = 0.00635\ \text{m}$, $G_{13}^c = 22.5914\ (\text{MPa})$, $G_{23}^c = 22.5914\ (\text{MPa})$, $\rho_c = 121.85\ (\text{Kg/m}^3)$. Other parameters such as the fiber orientation and layup of the facings, the nondimensional damping parameter, and the uniform pressure are given, respectively, as $[0/\text{Core}/0]$, $\Delta = 0$, $q_0 = 61.6\ \text{Pa}$ and $123.2\ \text{Pa}$. From Fig. 3, it can be seen that close agreement exists. It should also be noted that for the incompressible core case $w_{mn}^d = 0$ which implies that $w_{mn}^a(t) = w_{mn}(t)$ which is constant throughout the thickness of the structure.

8.2 Present Results

For the present results, unless stated otherwise, the following geometrical and material properties are given, respectively, for the face-sheets as $t_f = 5\text{mm}$, $L_1 = L_2 = 900\text{mm}$, $E_1^f = 207\ (\text{GPa})$, $E_2^f = 5.17\ (\text{GPa})$, $G_{12}^f = 2.55(\text{GPa})$, $v_{12}^f = 0.25$, and $\rho_f = 1{,}588.22(\text{Kg/m}^3)$. The corresponding properties for the core are provided as $t_c = 50\text{mm}$, $E_3^c = 3\ (\text{GPa})$, $G_{13}^c = 0.1027\ (\text{GPa})$, $G_{23}^c = 0.0621\ (\text{GPa})$, $\rho_c = 16\ (\text{Kg/m}^3)$. Other parameters such as the fiber orientation and layup of the facings, the nondimensional damping parameter, the peak

overpressure q_{s0}, the ambient pressure q_0, the positive phase duration t_p, and the rate of decay α are given, respectively, as $[0/\text{Core}/0]$, $\Delta = 0.05$, $q_{s0} = 1.766(\text{MPa})$, $q_0 = 101(\text{KPa})$, $t_p = 0.001372(\text{sec})$, and $\alpha = 0.5$. It is also assumed that the time of arrival, $t_a = 0$ or that the time of the blast begins at $t = 0$.

The present results begin with Fig. 4 and 5. depicting the effect of the transverse modulus of the core on the global and wrinkling response of the sandwich panel. It should be clarified that the terms global and wrinkling response will be refered to throughout the analysis of the results. The global response is a measure given by the average of the top and bottom face sheet deflection-time histories and is measured by $w_{mn}^{a}(t)$. While, the wrinkling (local) response gives a measure of half of the difference between the top and bottom face sheets with regards to the deflection-time histories, $w_{mn}^{d}(t)$. It should be noted that in the case of the incompressible core, $w_{mn}^{d}(t) = 0$. Also, in sandwich structural applications the goal from a design standpoint is to contain or limit the amount of wrinkling that occurs within the structure. With this in mind, It is revealed, in Figs. 4 and 5, that for larger values of the young's modulus of the core the effect on the global response is minimal. Whereas, for the case of the wrinkling response in Fig. 5, the effects upon the deflection-time histories appears to be more beneficial as a result of the decreased amplitudes of deflection.

In Fig. 6, it can be seen that for larger rates of decay that the global deflection-time history response remains for longer periods of time within the negative phase or suction phase of the blast pulse. In Fig 7, which is the counterpart of Fig. 6 for the case of the wrinkling response it is shown that a similar trend is observed as in Fig. 6. In addition, it appears that the frequencies are larger for both cases as the rate of decay is increased.

Fig. 8 shows that global deflection-time response is enhanced with the thicker core from the standpoint of decreased amplitudes of deflection. Also the frequency of the deflection-time response begins to grow out of phase with the thinner core revealing a larger frequency of oscillation. The same behavior can be seen in Fig. 9 which is the counterpart of Fig. 8 concerned with the wrinkling response.

Fig. 10 presents the effect of the stacking sequences and the increase in thickness of the facings. It can be seen that the cross-ply layup coupled with an increase in the face thickness greatly enhances the structural response. It is also observed that the cross-ply layup with increased thickness is a little out of phase with the orthotropic single layered facings. The same analysis also holds true for the wrinkling response. It appears that for the cross-ply layup with increased face thickness, that the wrinkling response is only marginally or negligibly affected.

In Figs. 12 and 13, it can be seen that the global response is more sensitive to the core transverse modulus ratio than the wrinkling response in Fig 13.

9. Concluding Remarks

The governing theory of asymmetric sandwich plates with a first-order compressible core impacted by a Friedlander-type of blast has been presented and simplified for the case of symmetric cross-ply and single-layered orthotropic facings. In all cases, it was mentioned that all four edges are simply supported and freely movable. Results were then presented for this simplified case and validated against results found in the literature from R. S. Alwar et al. [1]. It was found that for the incompressible core case that there was close agreement among the results. In regards to the compressible core case, no appropriate results have been found in the literature for the theory presented in this paper for the simply supported case with all edges freely movable. The effect of a number of important geometrical and material parameters were

analyzed with conclusions drawn. Some of the important conclusions were that wrinkling response seems to be diminished as the young's modulus of the core is increased. The same is the case for larger rates of decay. Also, for thicker cores, both the global and wrinkling responses are less severe. It was also revealed that the compressibility of the core has only a marginal effect upon the global response of the sandwich plate. Finally, the cross-ply type layup when compared with single-layered facings seemed to have a large effect on the global response and less effect on the wrinkling response.

One should keep in mind that both the stress and strain profiles should be determined to determine possible failure of the structure.

Acknowledgement

The author would like to express thanks to the U.S. Army-RDECOM-TARDEC for their support and funding under the Independent Laboratory In-house Research program (ILIR).

Disclaimer

Reference herein to any specific commercial company, product, process, or service by trade name, trademark, manufacturer, or otherwise, does not necessarily constitute or imply its endorsement, recommendation, or favoring by the United States Government or the Department of the Army (DoA). The opinions of the authors expressed herein do not necessarily state or reflect those of the United States Government or the DoA, and shall not be used for advertising or product endorsement purposes.

Appendix A. Strain-Displacement Components

Strain-Displacement components for the face-sheets

$$\bar{\gamma}^a_{11} = u^a_{1,1} + \frac{1}{2}(u^a_{3,1})^2 + \frac{1}{2}(u^d_{3,1})^2$$

$$\bar{\gamma}^a_{22} = u^a_{2,2} + \frac{1}{2}(u^a_{3,2})^2 + \frac{1}{2}(u^d_{3,2})^2$$

$$\bar{\gamma}^a_{12} = \frac{1}{2}u^a_{1,2} + \frac{1}{2}u^a_{2,1} + \frac{1}{2}u^a_{3,1}u^a_{3,2} + \frac{1}{2}u^d_{3,1}u^d_{3,2}$$

$$\bar{\gamma}^d_{11} = u^d_{1,1} + u^a_{3,1}u^d_{3,1}$$

$$\bar{\gamma}^d_{22} = u^d_{2,2} + u^a_{3,2}u^d_{3,2}$$

$$\bar{\gamma}^d_{12} = \frac{1}{2}u^d_{1,2} + \frac{1}{2}u^d_{2,1} + \frac{1}{2}u^a_{3,1}u^d_{3,2} + \frac{1}{2}u^a_{3,2}u^d_{3,1}$$

The bending strains for the face sheets

$$\kappa^a_{11} = -u^a_{3,11}$$

$$\kappa^a_{22} = -u^a_{3,22}$$

$$\kappa^a_{12} = -u^a_{3,12}$$

$$\kappa^d_{11} = -u^d_{3,11}$$

$$\kappa^d_{22} = -u^d_{3,22}$$

$$\kappa^d_{12} = -u^d_{3,12}$$

Strain-Displacement components for the Core

$$\bar{\gamma}^c_{13} = -\frac{1}{t_c}u^d_1 + \left(\frac{2t_c + t^t_f + t^b_f}{4t_c}\right)u^a_{3,1} + \left(\frac{t^t_f - t^b_f}{4t_c}\right)u^d_{3,1} - \frac{1}{t_c}u^d_3 u^a_{3,1}$$

$$\bar{\gamma}^c_{23} = -\frac{1}{t_c}u^d_2 + \left(\frac{2t_c + t^t_f + t^b_f}{4t_c}\right)u^a_{3,2} + \left(\frac{t^t_f - t^b_f}{4t_c}\right)u^d_{3,2} - \frac{1}{t_c}u^d_3 u^a_{3,2}$$

$$\bar{\gamma}^c_{33} = -\frac{2}{t_c}u^d_3 + \frac{2}{t^2_c}(u^d_3)^2$$

$$\kappa^c_{13} = -\frac{1}{t_c}u^d_{3,1} + \frac{2}{t^2_c}u^d_3 u^d_{3,1} + \frac{4}{t^2_c}\Phi^c_1$$

$$\kappa_{23}^{c} = -\frac{1}{t_c} u_{3,2}^{d} + \frac{2}{t_c^2} u_3^{d} u_{3,2}^{d} + \frac{4}{t_c^2} \Phi_2^{c}$$

$$\kappa_{33}^{c} = 0$$

Appendix B. Constants

$$C_1 = C_3 = \frac{(\mu_n^a)^2 [A_{11}^f A_{22}^f - (A_{12}^f)^2]}{32(\lambda_m^2)^2 A_{11}^f}$$

$$C_2 = C_4 = \frac{(\lambda_m)^2 [A_{11}^f A_{22}^f - (A_{12}^f)^2]}{32(\mu_n)^2 A_{22}^f}$$

$$A_1 = \frac{-\frac{\lambda_m}{2}\left(\lambda_m^2 A_{11}^f - A_{12}^f \mu_n^2 + \frac{G_{xz}^c}{t_c}\right)}{4\lambda_m^2 A_{11}^f + \frac{2G_{xz}^c}{t_c}}$$

$$B_1 = \frac{-\frac{\mu_n}{2}\left(\mu_n^2 A_{22}^f - \lambda_m^2 A_{12}^f + \frac{G_{yz}^c}{t_c}\right)}{4\mu_n^2 A_{22}^f + \frac{2G_{yz}^c}{t_c}}$$

A_2, B_2 are determined from the following system of linear equations:

$$\begin{pmatrix} M_2 & M_3 \\ M_3 & M_4 \end{pmatrix} \begin{pmatrix} A_2 \\ B_2 \end{pmatrix} = \begin{pmatrix} R_2 \\ R_3 \end{pmatrix}$$

where

$$M_2 = 4\left(\lambda_m^2 A_{11}^f + \mu_n^2 A_{66}^f - \frac{G_{xz}^c}{2t_c}\right)$$

$$M_3 = 4\lambda_m \mu_n (A_{12}^f + A_{66}^f)$$

$$M_4 = 4\left(\lambda_m^2 A_{66}^f + \mu_n^2 A_{22}^f - \frac{G_{yz}^c}{2t_c}\right)$$

$$R_2 = \frac{\lambda_m}{2}\left(\lambda_m^2 A_{11}^f + (A_{12}^f + 2A_{66}^f)\mu_n^2 + \frac{G_{xz}^c}{t_c}\right)$$

$$R_3 = \frac{\mu_n}{2}\left(\mu_n^2 A_{22}^f + (A_{12}^f + 2A_{66}^f)\lambda_m^2 + \frac{G_{yz}^c}{t_c}\right)$$

$$\begin{pmatrix} M_5 & M_6 \\ M_6 & M_7 \end{pmatrix}\begin{pmatrix} A_3 \\ B_3 \end{pmatrix} = \begin{pmatrix} R_4 \\ R_5 \end{pmatrix}$$

where

$$M_5 = \lambda_m^2 A_{11}^f + \mu_n^2 A_{66}^f + \frac{2G_{xz}^c}{t_c}$$

$$M_6 = \lambda_m \mu_n (A_{12}^f + A_{66}^f)$$

$$M_7 = \mu_n^2 A_{22}^f + \lambda_m^2 A_{66}^f + \frac{2G_{yz}^c}{t_c}$$

$$R_4 = \frac{2a\lambda_m G_{xz}^c}{t_c}$$

$$R_5 = \frac{2a\mu_n G_{yz}^c}{t_c}$$

$$D_1 = -\frac{\lambda_m^2}{8}$$

$$D_2 = \frac{A_{12}^f \mu_n^2 - A_{11}^f \lambda_m^2}{16\lambda_m A_{11}^f}$$

$$D_3 = \frac{\lambda_m}{16}$$

$$E_1 = -\frac{\mu_n^2}{8}$$

$$E_2 = \frac{A_{12}^f \lambda_m^2 - A_{22}^f \mu_n^2}{16 \mu_n A_{22}^f}$$

$$E_3 = \frac{\mu_n}{16}$$

Appendix C. Elastic Coefficients

$$C_{10}^a = \lambda_m^4 D_{11}^f + 2\lambda_m^2 \mu_n^2 (D_{12}^f + 2D_{66}^f) + \mu_n^4 D_{22}^f + \frac{2a\lambda_m G_{xz}^c}{t_c}(a\lambda_m - A_3) + \frac{2a\mu_n G_{yz}^c}{t_c}(a\mu_n - B_3)$$

$$C_{11}^a = -\frac{32}{9\pi^2}\left[2\lambda_m^3 A_{11}^f A_3 + \lambda_m \mu_n (A_{66}^f + 2A_{12}^f)(\lambda_m B_3 + \mu_n A_3) + 2\mu_n^3 A_{22}^f B_3 - \frac{2a}{t_c}(\lambda_m^2 G_{xz}^c + \mu_n^2 G_{yz}^c)\right]$$
$$+ \frac{64a}{9\pi^2 t_c}\left[\lambda_m G_{xz}^c (A_2 - 3A_1) + \mu_n G_{yz}^c (B_2 - 3B_1)\right]$$

$$C_{12}^a = 2\lambda_m^2 \mu_n^2 (C_1 + C_2) + \frac{\lambda_m^3 A_{11}^f}{16}\left[3\lambda_m + 8(A_2 - 2A_1)\right] + \frac{\mu_n^3 A_{22}^f}{16}\left[3\mu_n + 8(B_2 - 2B_1)\right] + \frac{\lambda_m \mu_n A_{12}^f}{8}\left[\right.$$
$$\left. 4\lambda_m (B_2 - 2B_1) + 4\mu_n (A_2 - 2A_1) + 3\lambda_m \mu_n\right] + \frac{\lambda_m \mu_n A_{66}^f}{4}\left[4(\mu_n A_2 + \lambda_m B_2) - \lambda_m \mu_n\right]$$

$$C_{30}^a = 2\lambda_m^2 \mu_n^2 (C_1 + C_2)$$

$$C_{01}^d = \lambda_m^4 D_{11}^f + 2\lambda_m^2 \mu_n^2 (D_{12}^f + 2D_{66}^f) + \mu_n^4 D_{22}^f + 2E^c$$

$$C_{02}^d = -\frac{128E^c}{3\pi^2 t_c}$$

$$C_{03}^d = 2\lambda_m^2 \mu_n^2 (C_1 + C_2) + \frac{9E^c}{4t_c^2}$$

$$C_{20}^d = -\frac{64}{9\pi^2}\left[\lambda_m^3 A_{11}^f A_3 + \lambda_m \mu_n A_{12}^f (\lambda_m B_3 + \mu_n A_3) + \mu_n^3 A_{22}^f B_3 + \frac{\lambda_m \mu_n A_{66}^f}{2}(\lambda_m B_3 + \mu_n A_3)\right]$$

$$C_{21}^d = \frac{1}{2}\left[\lambda_m^3 A_{11}^f\left(A_2 - 2A_1 + \frac{3\lambda_m}{8}\right) + \lambda_m \mu_n A_{12}^f\left[\mu_n (A_2 - 2A_1) + \lambda_m (B_2 - 2B_1) + \frac{3}{4}\lambda_m \mu_n\right] +\right.$$
$$\left. \mu_n^3 A_{22}^f\left(B_2 - 2B_1 + \frac{3}{8}\mu_n\right) + 2\lambda_m \mu_n A_{66}^f\left(\mu_n A_2 + \lambda_m B_2 - \frac{1}{4}\lambda_m \mu_n\right) + 4\lambda_m^2 \mu_n^2 (C_1 + C_2)\right]$$

References

[1] Alwar, R. S., and Adimurthy, N. K., "Non-Linear Dynamic Response of Sandwich Panels Under Pulse and Shock Type Excitations", *Journal of Sound and Vibration*, Vol. 39(1), Pgs. 43-54, 1975.

[2] Deshpande, V. S., and Fleck, N. A., "One-Dimensional Response of Sandwich Plates to Underwater Shock Loading", *Journal of Physics and Solids*, Vol. 53, Pgs. 2347-2383, 2005.

[3] Hause, T., and Librescu, L., "Dynamic Response of Doubly-Curved Anisotropic Sandwich Panels Impacted by Blast Loadings", *International Journal of Solids and Structures,* Vol 44, Issue 20, pp. 6678-6700, October 1, 2007.

[4] Hause, T., and Librescu, L., "Dynamic Response of Anisotropic Sandwich Flat Panels To Explosive Pressure Pulses", *Int J. of Impact Engineering*,Vol 31, pp. 607-628, 2005.

[5] Hohe, J. and Librescu, L., "A nonlinear theory for doubly curved anisotropic sandwich shells with transversely compressible core", *International Journal of Solids and Structures*, Vol. 40, Pgs 1059-1088, 2003.

[6] Hohe, J. and Librescu, L., "Recent Results on the Effect of the Transverse Core Compressibility on the Static and Dynamic Response of Sandwich Structures", *Composites: Part B*, Vol. 39, Pgs 108-119, 2008.

[7] Hohe, J. and Librescu, L., "Advances in the structural modeling of Elastic Sandwich Panels", *Mechanics of Advanced Materials and Structures* , Vol. 11, Pgs 395-424, 2004.

[8] Kingery, C.N. and G. Bulmash, "Air-Blast Parameters from TNT Spherical Airburst and Hemispherical Surface Burst", ABRL-TR-02555, U.S. Army Ballistic Research Laboratory, Aberdeen Proving Ground, MD, April 1984.

[9] Liang, Y., Spuskanyuk, A. V., Flores, S. E., Hayhurst, D. R., Hutchinson, J. W., McMeeking, R. M., and Evans, A. G., "The Response of Metallic Sandwich panels to Water Blast", *ASME Journal of Applied Mechanics*, Vol. 74, Pgs. 81-99.

[10] Librescu, L., "Linear and Non-Linear Dynamic Response of Sandwich Panels to Blast Loading", *Composites: Part B*, Vol. 35B, Issue 6-8, Pgs 673-683, 2004.

[11] Librescu, L., Yong S., and Hohe J., "Dynamic Response of Anisotropic Sandwich Flat Panels to Underwater and in-Air Explosions", *International Journal of Solids and Structures*, Vol. 43, Pgs 3794-3816, 2006.

[12] Librescu, L., Yong S., and Hohe J., "Implication of Nonclassical Effects on Dynamic Response of Sandwich Structures Exposed to Underwater and in-Air Explosions", *Journal of Ship research*, Vol. 51, No. 2, Pgs 83-93, 2007.

[13] Nemat-Nassar, S., Kang, W. J., McGee, J. D., Guo, W. G., and Issacs, J. B., "Experimental Investigation of Energy-Absorption Characteristics of Components of Sandwich Structures", *International Journal of Impact Engineering*, Vol. 34, Pgs. 1119-1146, 2007.

[14] Renfu, L., Kardomateas, G.A., and Simitses, G.J., "Nonlinear Response of a Shallow Sandwich Shell with Compressible Core to Blast Loading", *Journal of Applied Mechanics*, Vol. 75, Pgs. 1-10, 2008.

[15] Renfu, L. and Kardomateas, G.A., "Nonlinear High-Order Theory for Sandwich Plates with Orthotropic Phases", *AIAA Journal*, Vol. 46, No. 11, Pgs. 1-10, November 2008.

[16] Reddy, J.N., "Mechanics of Laminated Composite Plates and Shells - Theory and Analysis", 2nd Edition, *CRC Press*, 1997.

[17] Xue, Z., and Hutchinson, J. W., "Preliminary Assessment of Sandwich Plates Subject to Blast Loads", *International Journal of Mechanical Sciences*, Vol. 45, Pgs. 687-705, 2003.

Figure Captions

Fig. 1 A depiction of an asymmetric sandwich plate under an in-air Friedlander explosion.

Fig. 2 Incident profile of the pressure-time relationship for a Friedlander-type blast.

Fig. 3 The nondimensional global deflection-time response for the case of an incompressible core impacted by a uniform pressure pulse

Fig. 4 The effect of the transverse modulus of the core on the global response of a sandwich plate with orthotropic facings.

Fig. 5 The counterpart of Fig. 4 for the wrinkling response of a sandwich plate.

Fig. 6 The effect of the rate-of-decay parameter on the global response of a sandwich plate with orthotropic facings.

Fig. 7 The counterpart of Fig. 6 for the wrinkling response.

Fig. 8 The effect of the core thickness on the global deflection-time history of a sandwich plate with orthotropic facings.

Fig. 9 The counterpart of Fig. 8 for the wrinkling response.

Fig. 10 The effect of the stacking sequence of the facings on the global response of a sandwich plate.

Fig. 11 The counterpart of Fig. 12 for the wrinkling response.

Fig. 12 The effect of the core shear modulus ratio on the deflection-time history of cross-ply laminated sandwich plate.

Fig. 13 The counterpart of Fig. 12 for the wrinkling response.

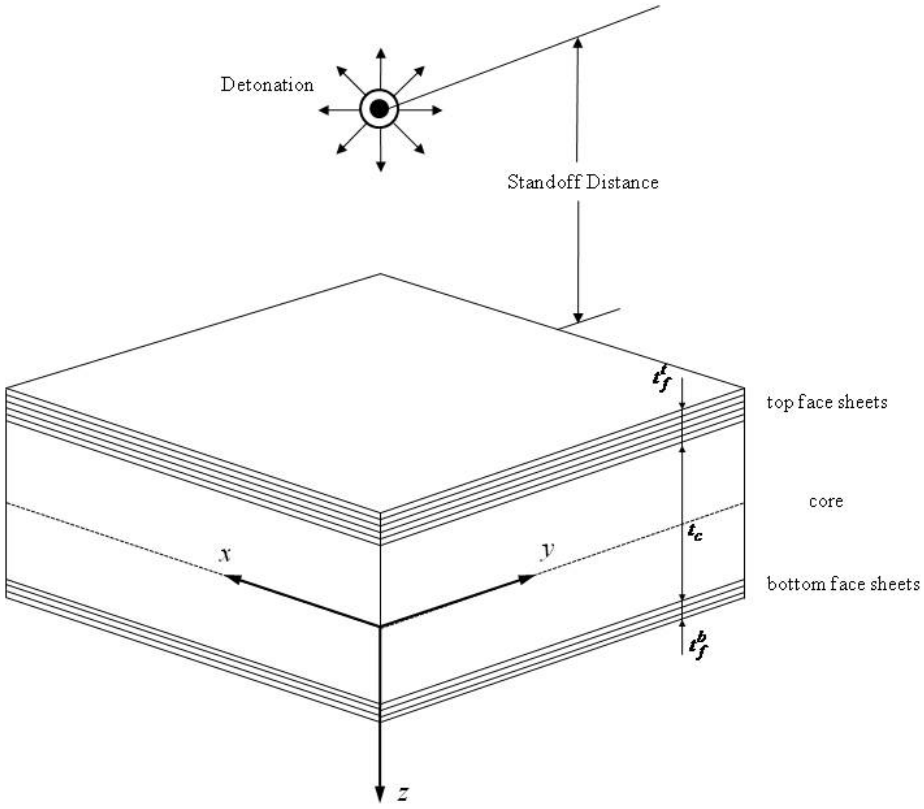
Detonation
Standoff Distance
t_f^t
top face sheets
core
t_c
x
y
bottom face sheets
t_f^b
z

Fig. 1

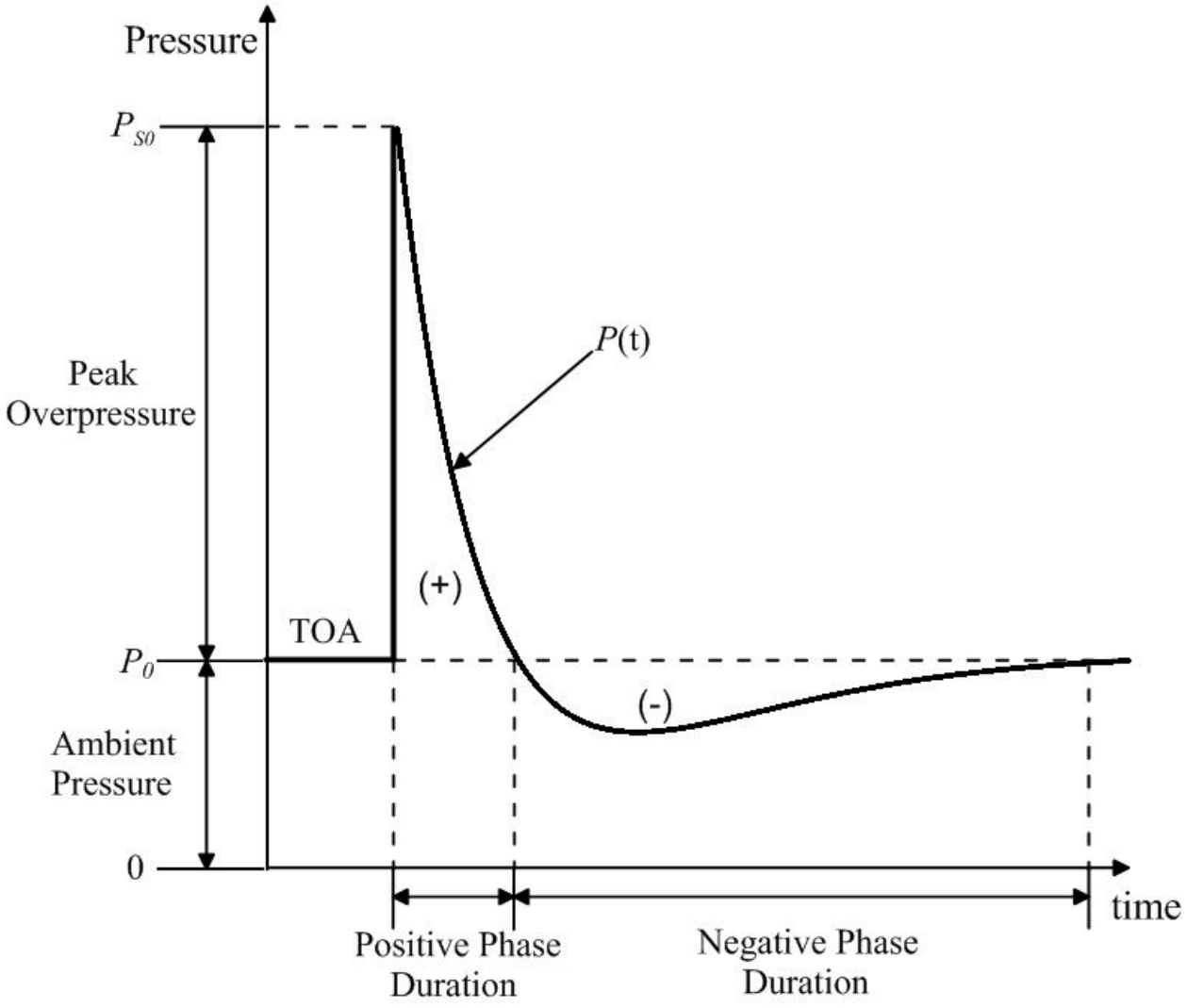
Pressure
P_{S0}
Peak
Overpressure
P(t)
(+)
TOA
P_0
(-)
Ambient
Pressure
0
time
Positive Phase
Duration
Negative Phase
Duration

Fig. 2

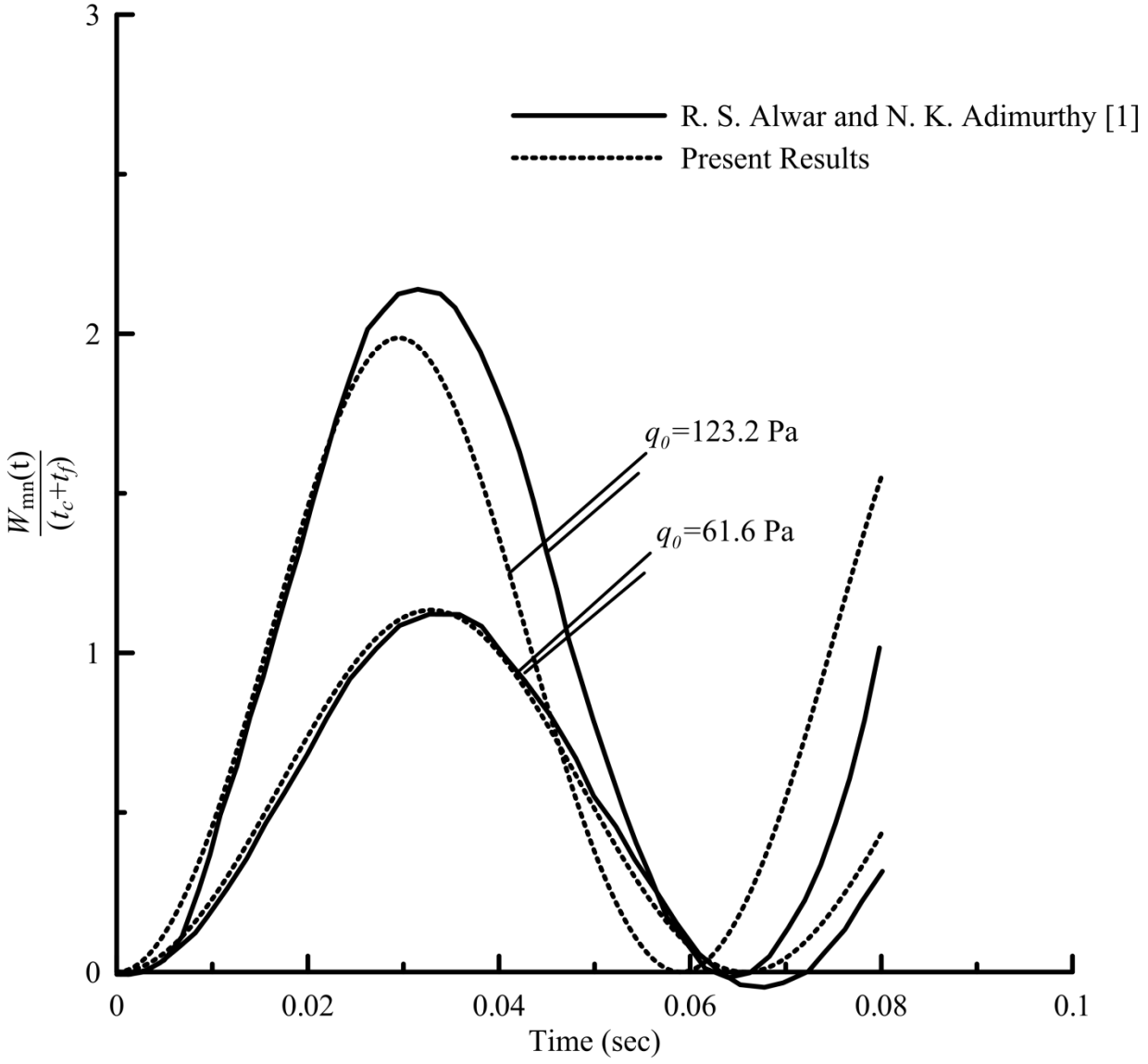
R. S. Alwar and N. K. Adimurthy [1]
Present Results
q_0=123.2 Pa
q_0=61.6 Pa
$\frac{W_{mn}(t)}{(t_c+t_f)}$
Time (sec)
0
1
2
3
0
0.02
0.04
0.06
0.08
0.1

Fig. 3

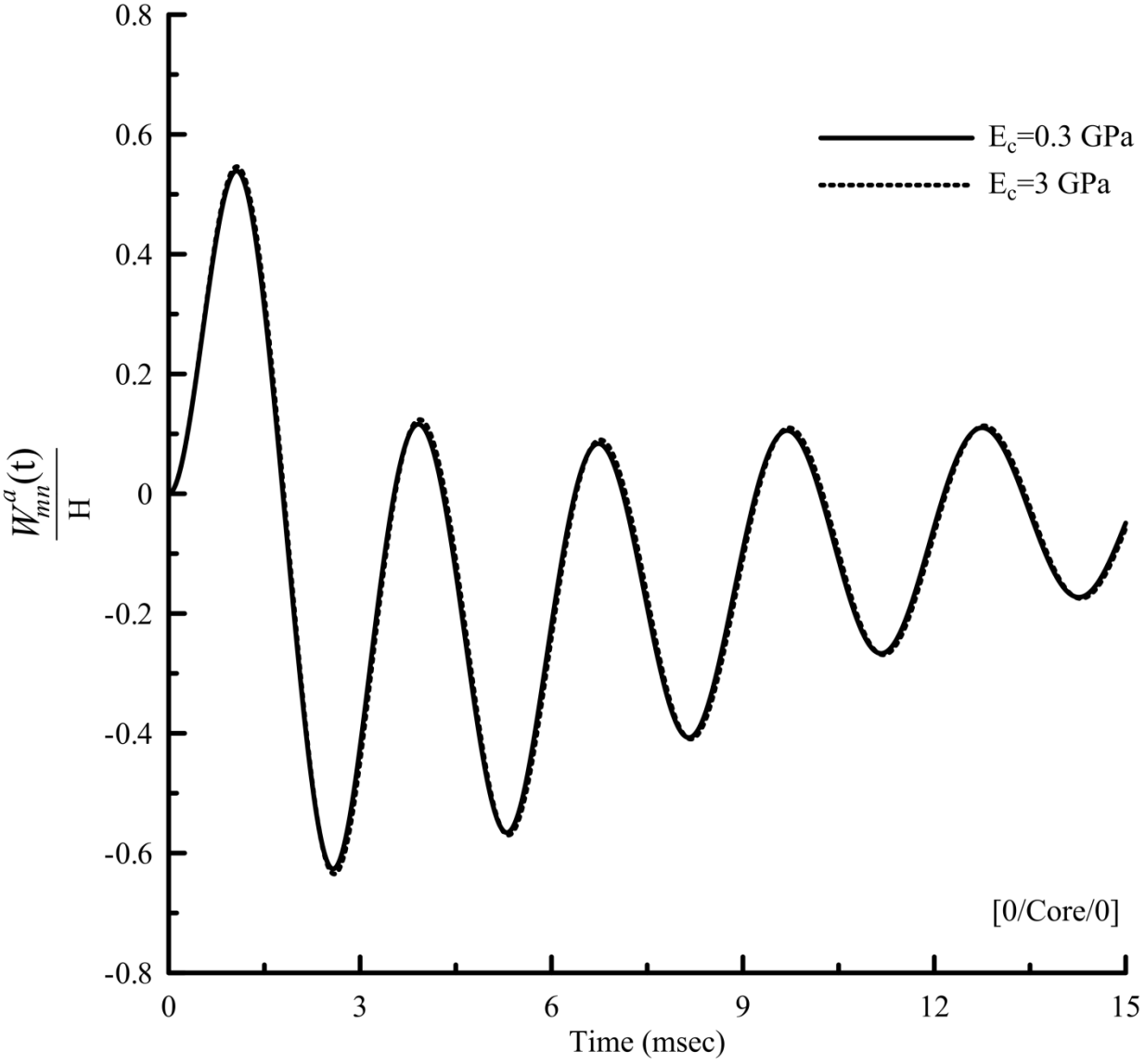
0.8
0.6
0.4
0.2
0
-0.2
-0.4
-0.6
-0.8
$\frac{W_{mn}^{a}(t)}{H}$
0
3
6
9
12
15
Time (msec)
E_c=0.3 GPa
E_c=3 GPa
[0/Core/0]

Fig. 4

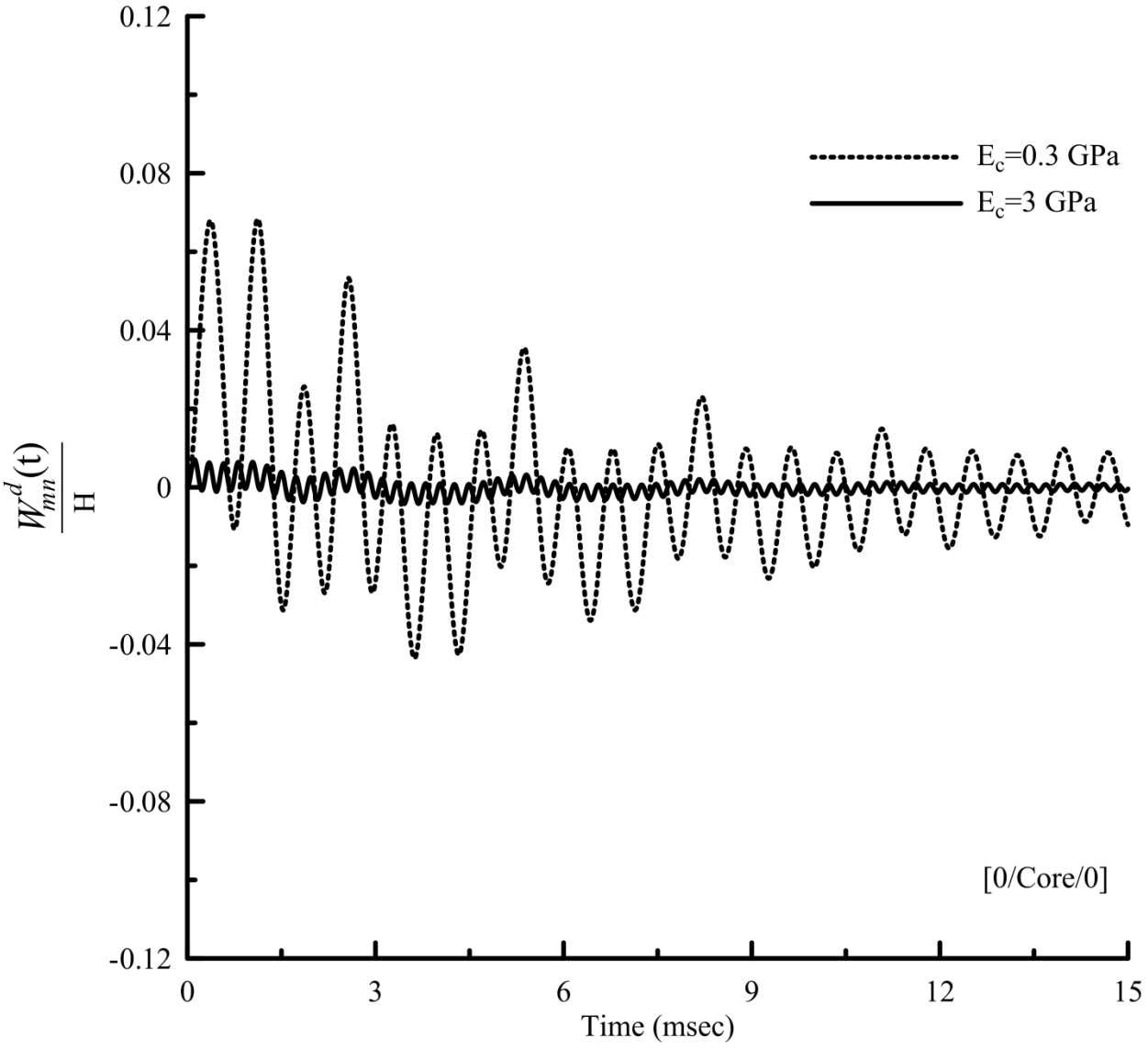
0.12
0.08
0.04
0
-0.04
-0.08
-0.12
$\frac{W_{mn}^{d}(t)}{H}$
E_c=0.3 GPa
E_c=3 GPa
[0/Core/0]
0
3
6
9
12
15
Time (msec)

Fig. 5

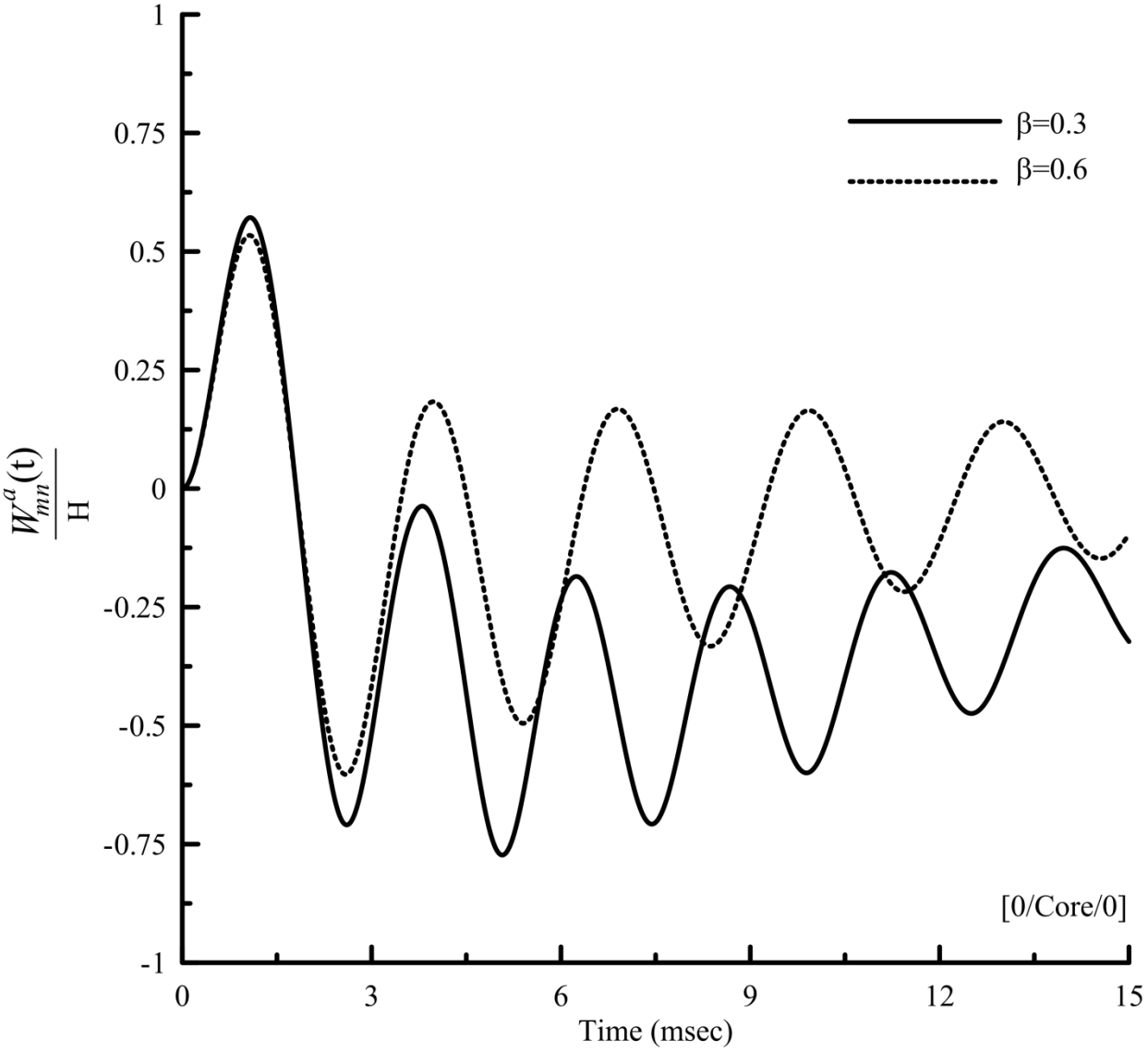
1
0.75
0.5
0.25
0
-0.25
-0.5
-0.75
-1
$\frac{W_{mn}^{a}(t)}{H}$
β=0.3
β=0.6
[0/Core/0]
0
3
6
9
12
15
Time (msec)

Fig. 6

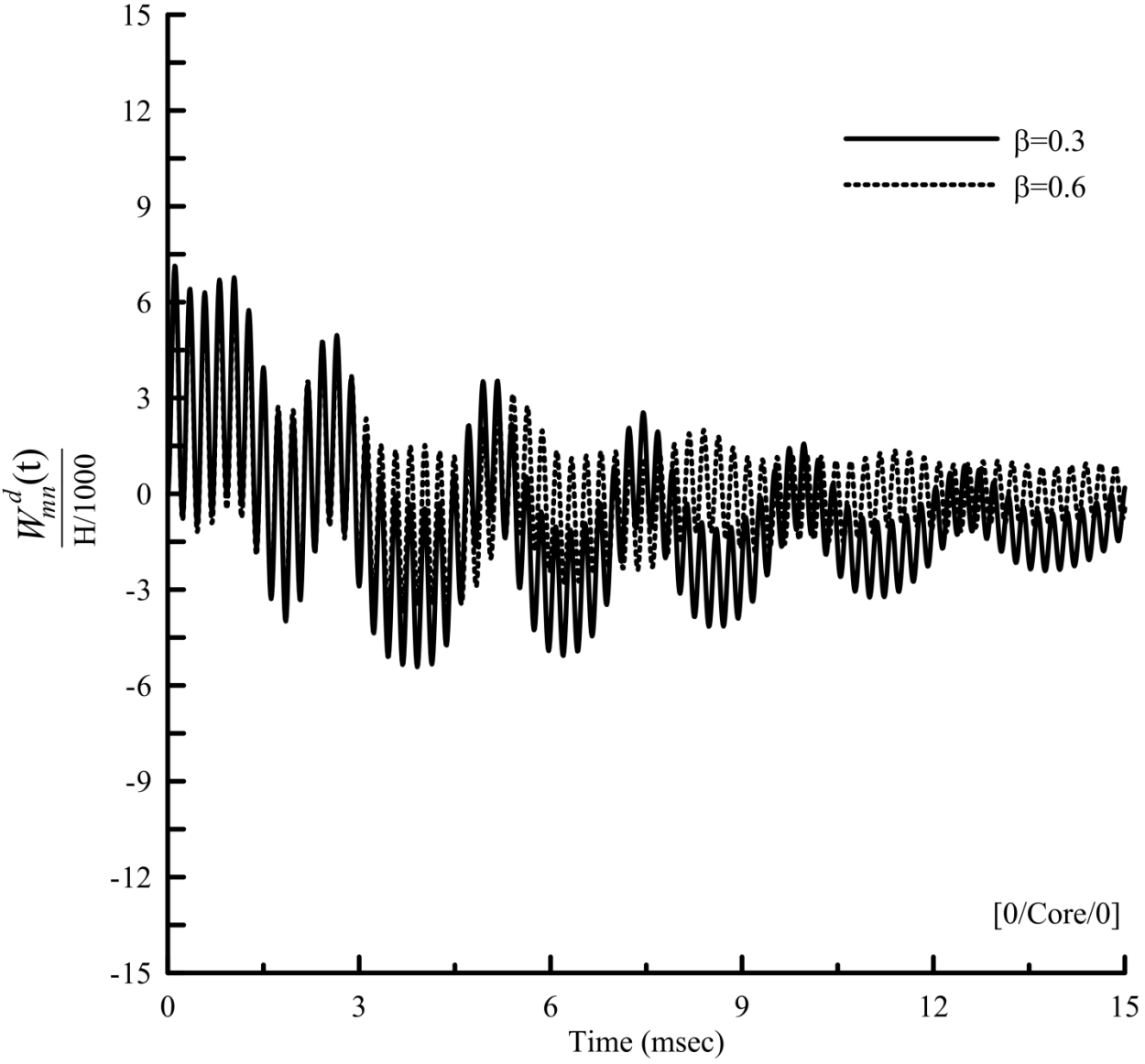
15
12
9
6
3
0
-3
-6
-9
-12
-15
0
3
6
9
12
15
Time (msec)
$\frac{W_{mn}^{d}(t)}{H/1000}$
β=0.3
β=0.6
[0/Core/0]

Fig. 7

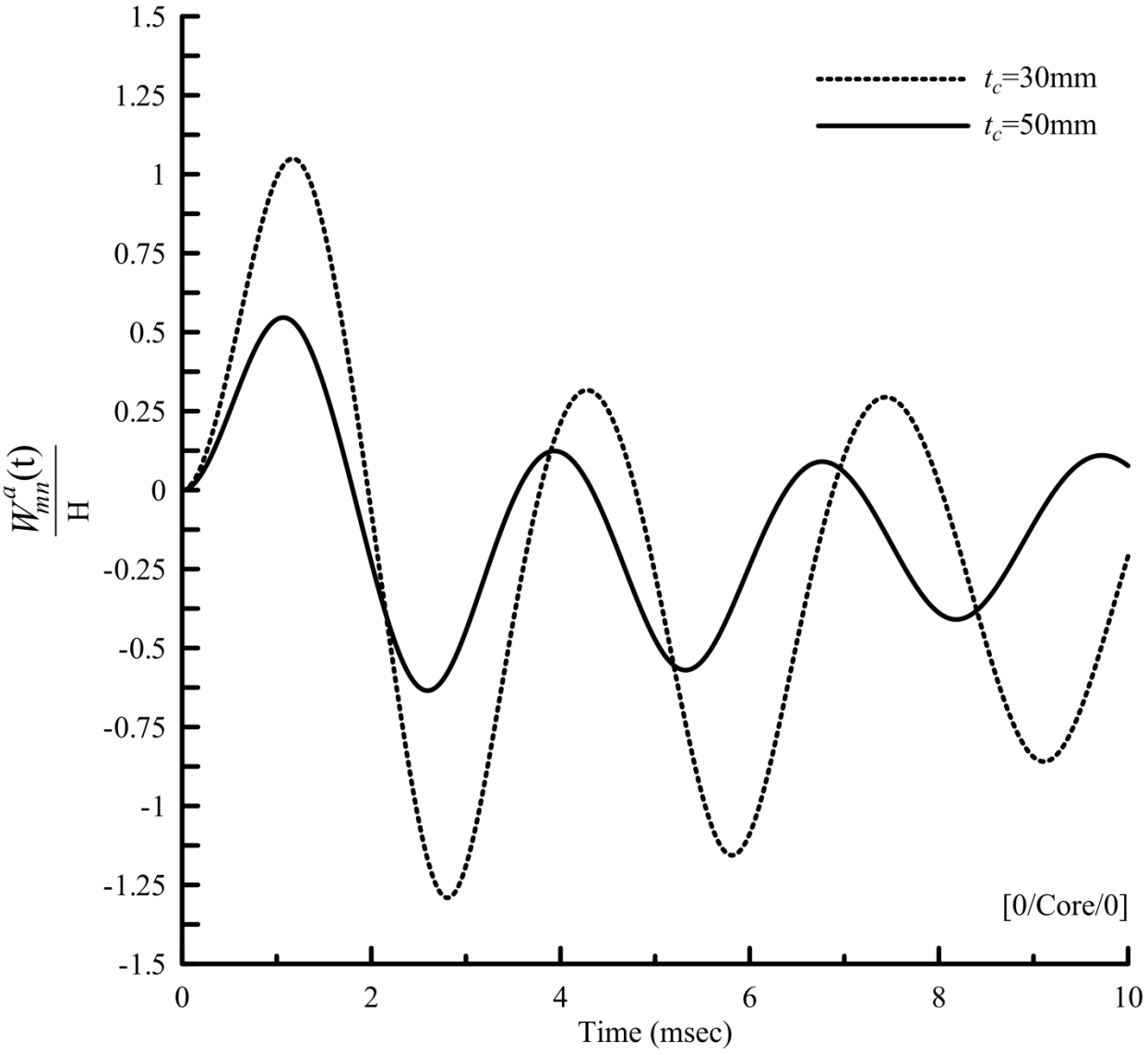
1.5
1.25
1
0.75
0.5
0.25
0
-0.25
-0.5
-0.75
-1
-1.25
-1.5
$\frac{W_{mn}^{a}(t)}{H}$
0
2
4
6
8
10
Time (msec)
t_c=30mm
t_c=50mm
[0/Core/0]

Fig. 8

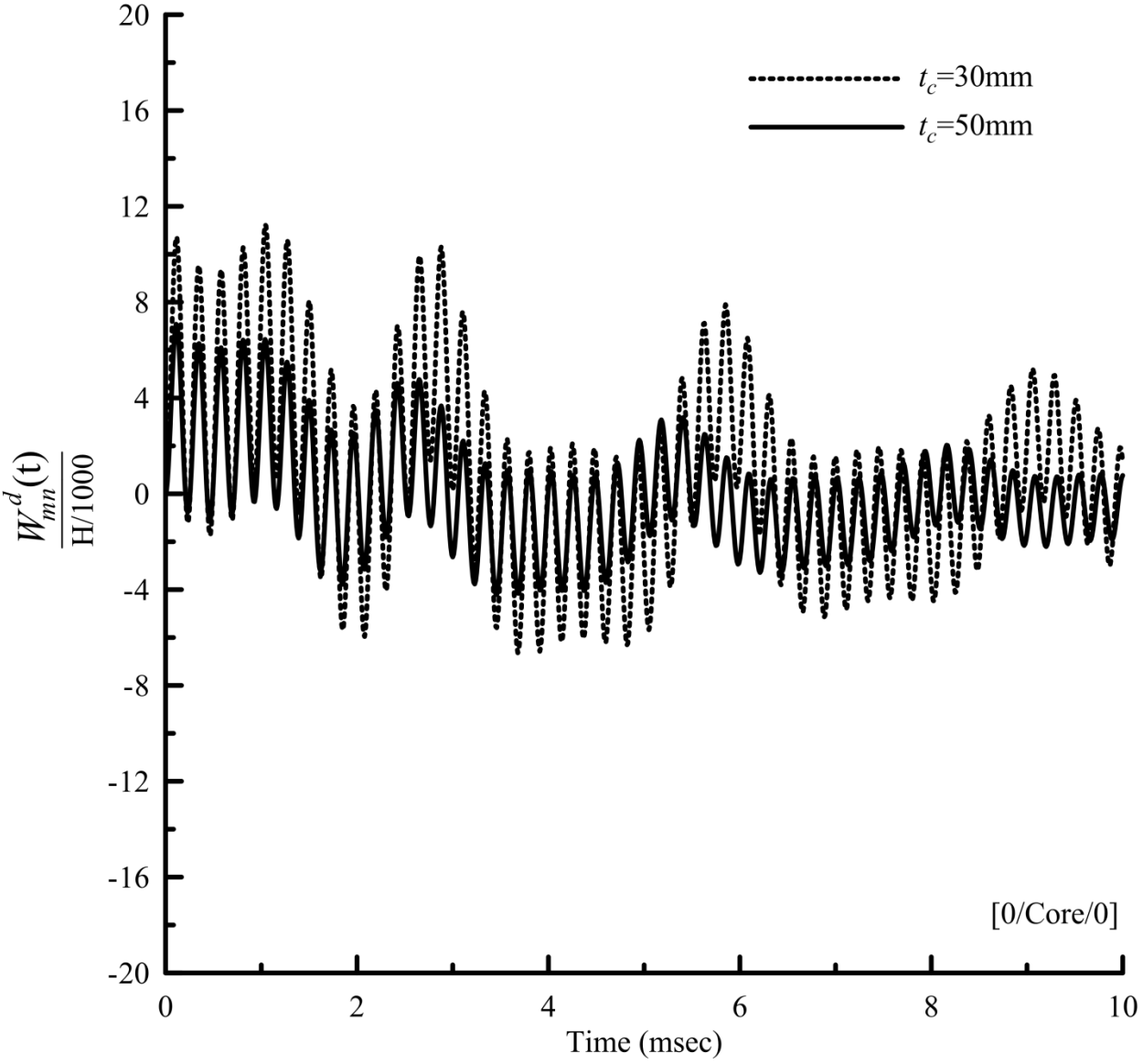
20
16
12
8
4
0
-4
-8
-12
-16
-20
0
2
4
6
8
10
Time (msec)
$\frac{W_{mn}^{d}(t)}{H/1000}$
t_c=30mm
t_c=50mm
[0/Core/0]

Fig. 9

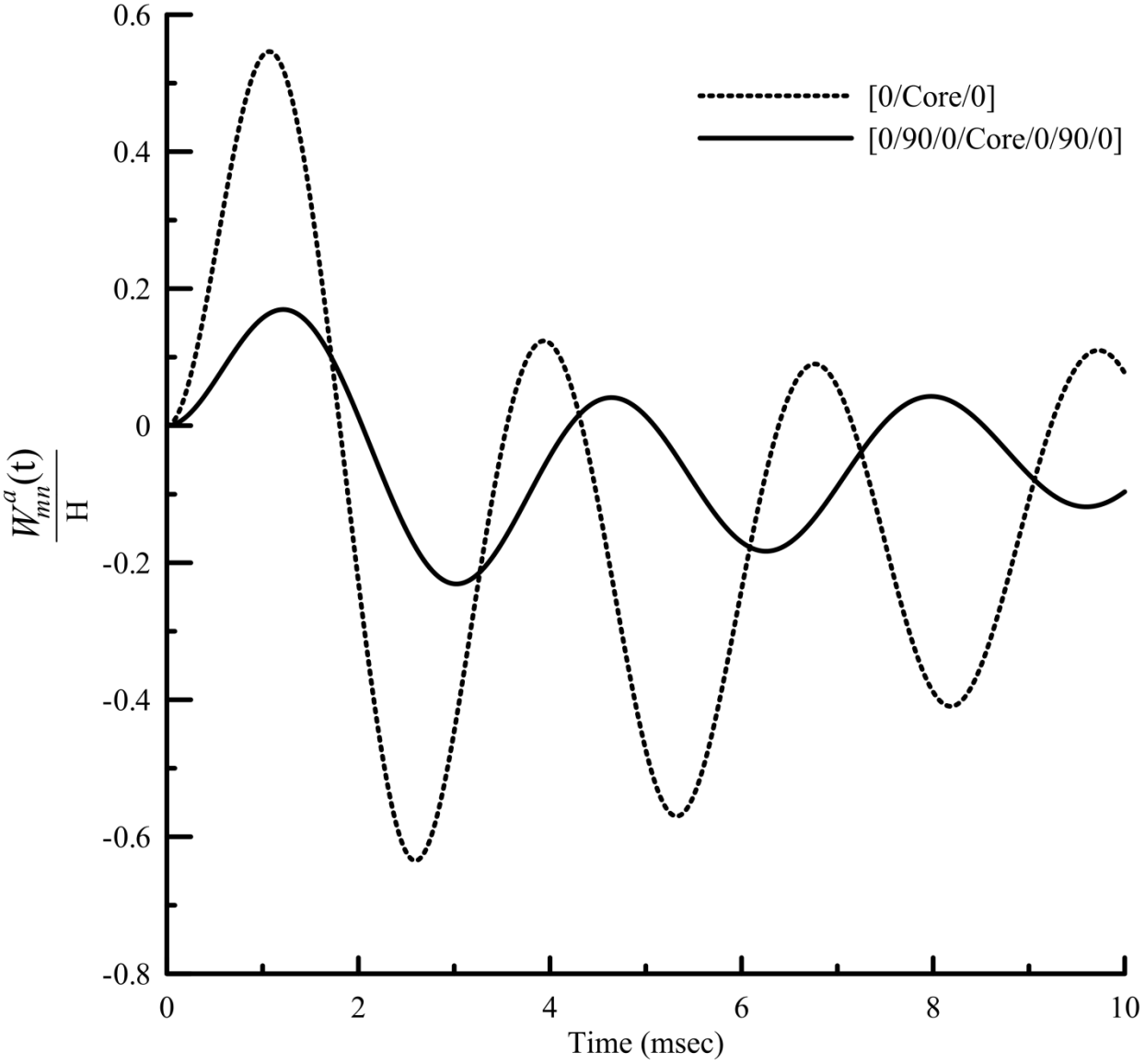
0.6
0.4
0.2
0
-0.2
-0.4
-0.6
-0.8
0
2
4
6
8
10
Time (msec)
$\frac{W_{mn}^{a}(t)}{H}$
[0/Core/0]
[0/90/0/Core/0/90/0]

Fig. 10

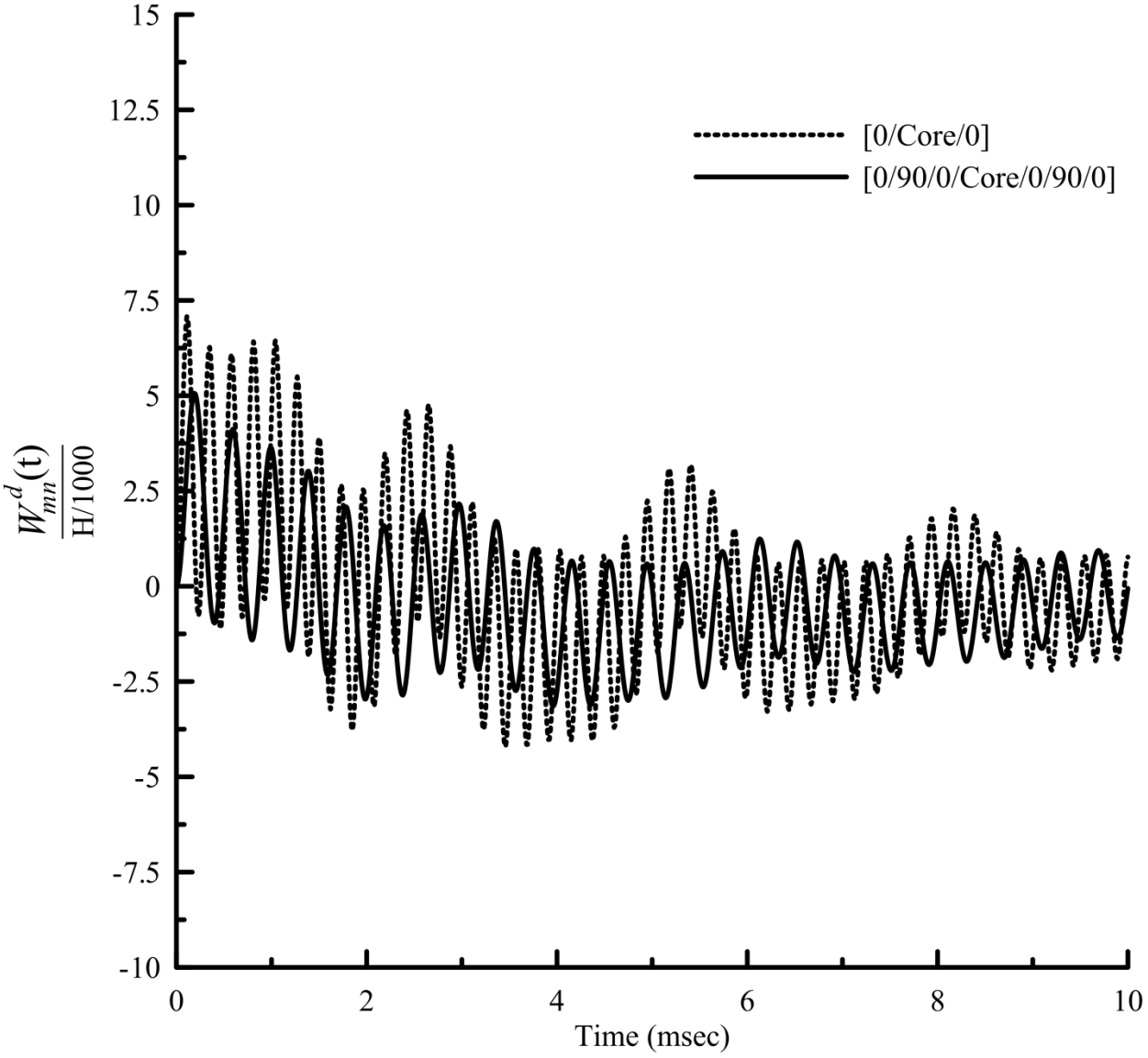
15
12.5
10
7.5
5
2.5
0
-2.5
-5
-7.5
-10
0
2
4
6
8
10
Time (msec)
$\frac{W_{mn}^{d}(t)}{H/1000}$
[0/Core/0]
[0/90/0/Core/0/90/0]

Fig. 11

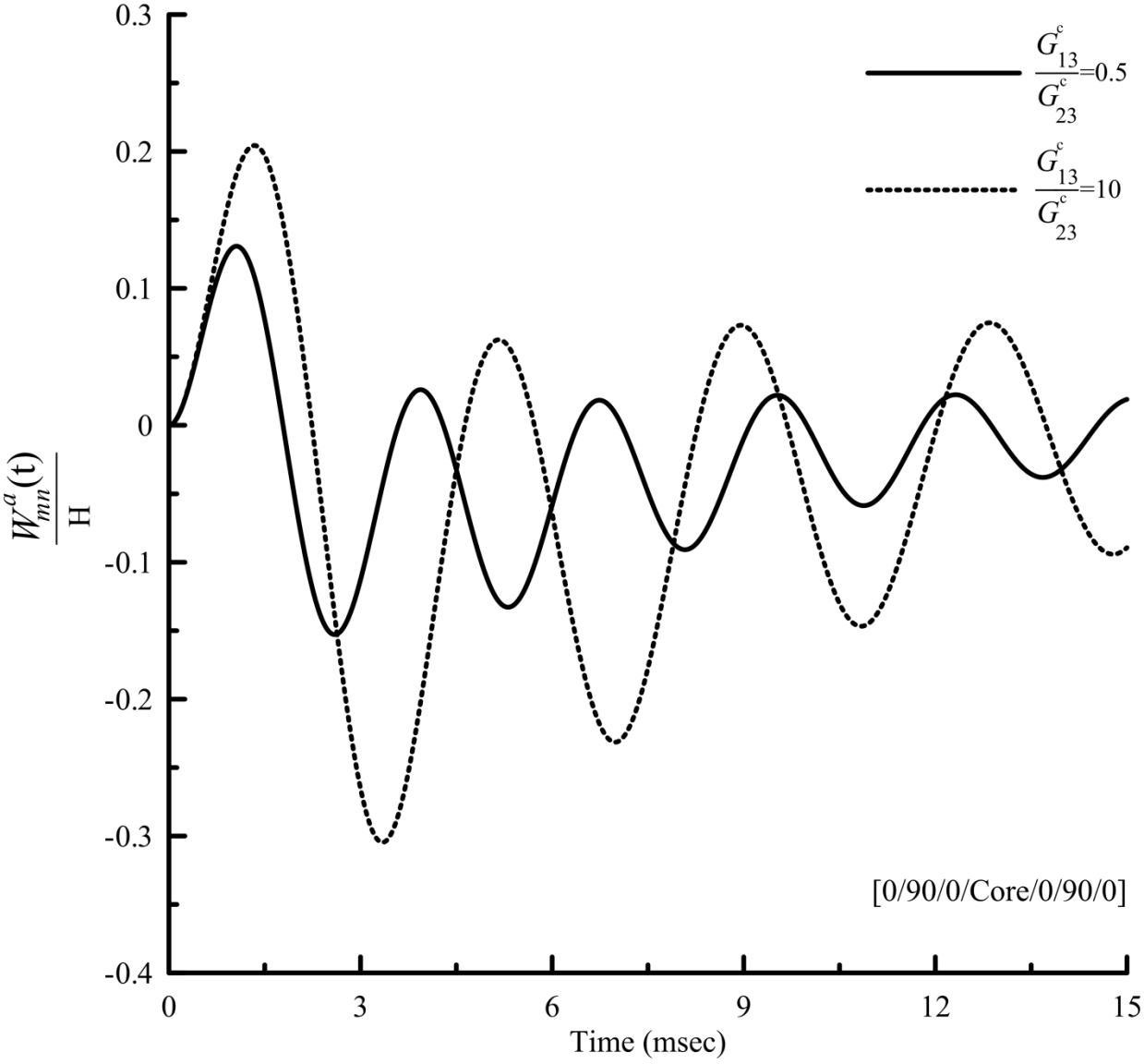
0.3
0.2
0.1
0
-0.1
-0.2
-0.3
-0.4
0
3
6
9
12
15
Time (msec)
$\frac{W_{mn}^{a}(t)}{H}$
$\frac{G_{13}^{c}}{G_{23}^{c}}$=0.5
$\frac{G_{13}^{c}}{G_{23}^{c}}$=10
[0/90/0/Core/0/90/0]

Fig. 12

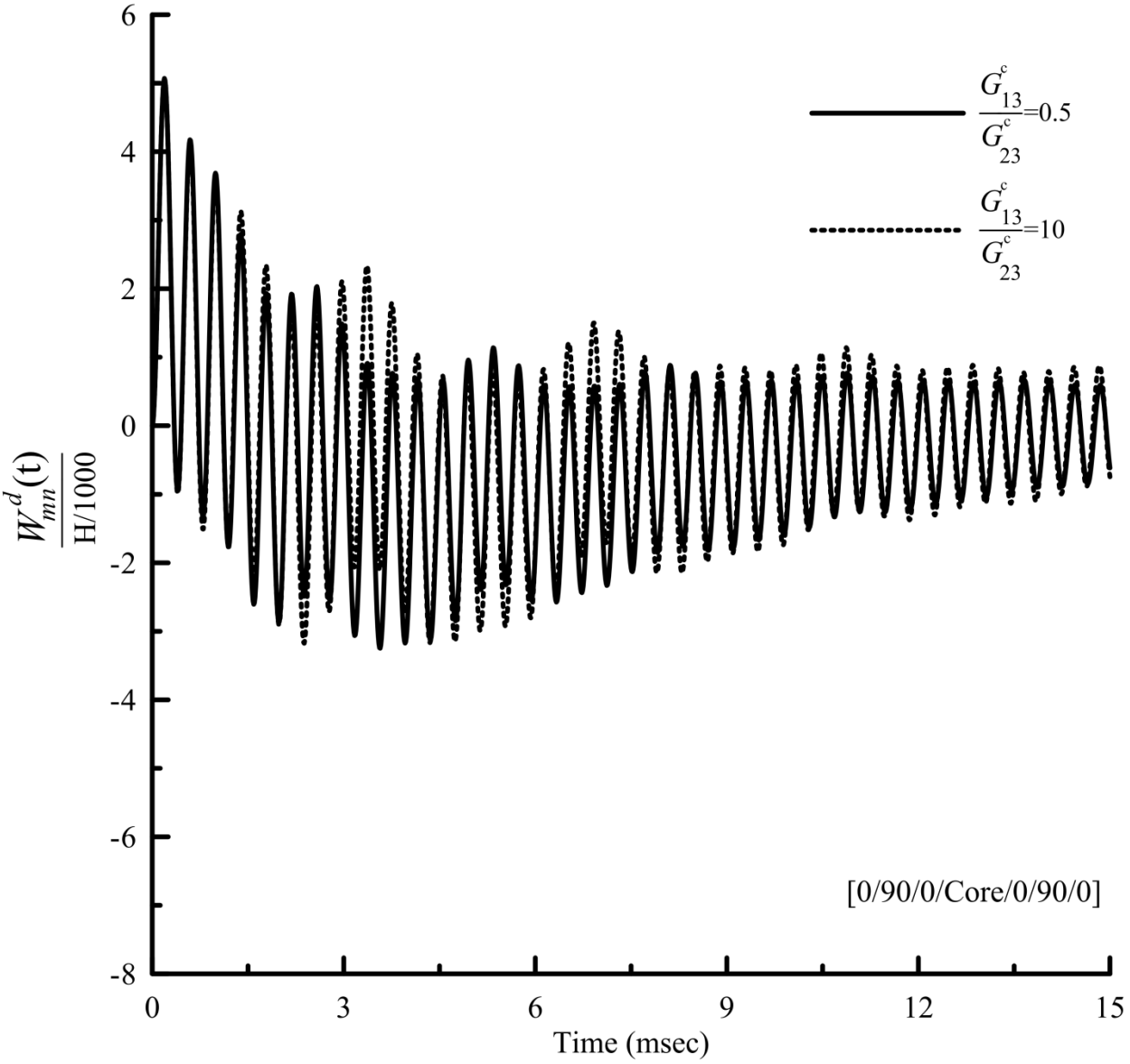
6
4
2
0
-2
-4
-6
-8
0
3
6
9
12
15
Time (msec)
$\frac{W_{mn}^{d}(t)}{H/1000}$
$\frac{G_{13}^{c}}{G_{23}^{c}}$=0.5
$\frac{G_{13}^{c}}{G_{23}^{c}}$=10
[0/90/0/Core/0/90/0]

Fig. 13